Doctoral Thesis

Computational Study of Stress Corrosion Cracking on Nickel Based Alloy Exposed to Water Environment

KwangBeom Ko

Department of Nuclear Engineering

Ulsan National Institute of Science and Technology

2021

Computational Study of Stress Corrosion Cracking on Nickel Based Alloy Exposed to Water Environment

KwangBeom Ko

Department of Nuclear Engineering

Ulsan National Institute of Science and Technology

Computational Study of Stress Corrosion Cracking on Nickel Based Alloy Exposed to Water Environment

A thesis/dissertation submitted to
Ulsan National Institute of Science and Technology
in partial fulfillment of the
requirements for the degree of
Doctor of Philosophy

KwangBeom Ko

07.12.2021 of submission

Approved by

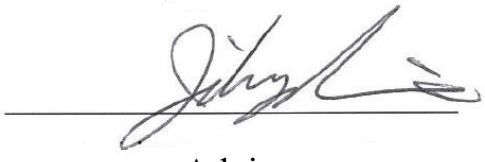

Advisor

Ji Hyun Kim

Computational Study of Stress Corrosion Cracking on Nickel Based Alloy Exposed to Water Environment

KwangBeom Ko

This certifies that the thesis/dissertation of KwangBeom Ko is approved.

07.12.2021 of submission

Signature

Advisor: Ji Hyun Kim

Signature

In Cheol Bang

Signature

Soon Yong Kwon

Signature

Eisung Yoon

Signature

Chi Bum Bahn

ABSTRACT

As the design life of nuclear power plants approaches, continued operation of nuclear power plants is emerging as a problem. For long-term operations, it is imperative that the safety should be guaranteed first. To this end, we need to be able to understand the underlying mechanisms of material degradation to predict the degradation of the components of nuclear power plants.

The nickel based alloys are pivotal structural materials used in nuclear industry because of corrosion resistance and mechanical properties that tolerate harsh and extreme environments. However, nickel based alloys undergo stress corrosion cracking (SCC) in high-temperature high-pressure environments. Stress corrosion cracking is a generic problem in high temperature waters, with most alloys employed suffering from cracking under some conditions. Among these conditions, the oxidation of nickel-based alloys can be regarded as the origin of the initiation of SCC, which is the main degradation process that induces failure of nuclear power plants.

However, due to the difficulty of experiments and theoretical analysis on high temperature and high pressure conditions, there remains uncertainty about over the underlying mechanism despite many decades of research. It is difficult to justify the continuous operation of nuclear power plants because the conditions in which these uncertainties exist lead to possible component problems due to degradation of materials.

In this thesis, computational approaches and X-ray experiments have been used to overcome traditional experimental and theoretical limitations on the primary water stress corrosion cracking of nickel based alloys to investigate the atomistic mechanism of phenomenon. The first principle method and molecular dynamics techniques have been applied to Ni/H_2O and Ni-15Cr-8Fe/H_2O systems as one of the ways to predict complex interactions between water and alloy elements. By the computational approach, the behavior of atoms including adsorption energy and barrier energy are evaluated and compared with results derived from conventional experimental methods.

Previous studies have shown that PWSCC is affected by a number of factors, but it is affected by alloy elements and changes in the composition of alloying elements change the oxidation behavior that occurs on the surface. However, a discrepancy between the various phase boundaries have been found in the oxide layer of the nickel based alloy surface and many consequences was effected by this phenomenon are not yet clear. Because, the oxidation layer properties on the oxidation of nickel in primary water is important to understand PWSCC, oxidation behavior analysis provides reliable oxidation layer phase boundary properties and compares with experimental data in this thesis.

First principle method, molecular dynamics and X-ray experimental techniques were used to analyze the early stage oxidation process on the nickel surface. In these early stage oxidation process models, potential is identified as a key parameter that should be verified in reactions caused by water on metal surfaces to assure reliable results. Developed for nickel-based alloys, the reactive force field potential is suitable for early stage oxidation process calculations and is used in many calculations where chemical reactions should be considered. The molecular dynamics techniques are used to identify discrepancies between phase changes and boundaries on surfaces and to verify them through X-ray experiments.

In this thesis, it has been proposed that the oxide layer was formed on the nickel substrate and structural changes occurred in the surface while the nickel was exposed to high temperature water environment. In the molecular dynamics results, oxygen atoms penetrate into the nickel substrate and interaction with nickel and chromium atoms. In addition to, this oxide layer is formed two types of the oxide layer. One is distorted crystal system and the other is amorphous layer by the interaction between oxygen and alloying elements atom. In X-ray experiments result show direct experimental evidence of co-existing amorphous and crystalline oxide phases within the film. This structural mismatch region can provide a diffusion path in which continuous phase change occurs. The oxygen atom can easily penetrate into the substrate and base metal suffer from accelerated mass transport due to vacancy or molecular structural change on the metal surface. This environment is promoted in which crack can be formed by providing conditions for creating a brittle oxide film inside the oxide layer. These damage processes are believed to play a major role in the initiation of cracks.

CONTENTS

LIST OF FIGURES

LIST OF TABLES

NOMENCLATURE

Abbreviations

NSSS	Nuclear Steam Supply System
IGSCC	Intergranular Stress Corrosion Cracking
XRR	X-Ray reflectivity
RHEED	Reflection High Energy Electron Diffraction
AFM	Atomic Force Microscopy
PWSCC	Primary Water Stress Corrosion Cracking
PWR	Pressurized Water Reactor
SCC	Stress Corrosion Cracking
MD	Molecular Dynamics
LAMMPS	Large-scale Atomic/Molecular Massively Parallel Simulator
XRD	X-Ray Diffraction
GIXR	Grazing Incidence X-Ray Reflectometry
HRXRD	High Resolution X-Ray Diffraction
ReaxFF	Reactive Force Field
DFT	Density Functional Theory
RDF	Radial Distribution Function

Greek Symbols

t_i	Crack Initiation Time
a_{cr}	Critical Depth
K_{ISCC}	Critical Stress Intensity Factor
σ	Applied Stress
u_f	Unit Vector of Reflected Beam Direction
u_i	Unit Vector of Incident Beam Direction
Λ	Linear Attenuation Length
η	Typical Per-Layer Attenuation Factor
n	Diffraction Order
λ	Wave Length
d	Bragg's Plane Spacing
θ	Incident Angle of X-ray
ε_j	Scattering Amplitudes
F	Structure Factor
f_0	Scattering Strength

1. INTRODUCTION

1.1. Background

Nickel based alloys are one of the most important structure materials in modern industries such as steam turbine power plants, aircraft gas turbine, chemical and nuclear industries because they have excellent performance of mechanical strength and corrosion resistance at high temperature aqueous environments [1]. Figure 1-1 shows a schematic illustration of applications of alloy 600 in pressurized water reactor primary system [2]. However, the interaction of nickel based alloys with water and oxygen atom causes dissolution of metallic atom and diffusion of elements. After then, oxidation arises at the surface.

Therefore, the formation of oxide layer is an unavoidable process in high temperature water environments. The oxidation process of metals and alloys is at the origin of the initiation of stress corrosion cracking(SCC). Almost all SCC on alloys in aqueous condition take place on their oxide films [3]. It can induce failure of structural materials. Hence, it is important to understand basic process of early stage of oxidation including dissociation process of water on alloys. Fig 1-2 is factor affecting stress corrosion cracking [4].

Early stage oxidation on the metals and alloys have been studied using various techniques [5-9], and many researches have been performed to understand and quantify the corrosion resistance of nickel base alloy by oxide analysis [10-14]. However, these experimental study not enough to reveal the oxidation and crack initiation process on atomic scale, which is fundamentally very important. Moreover, in detailed information on atomic scale is important to study corrosion and passivation phenomena.

Computational methods are a very powerful and reliable tool to overcome experimental barrier for understanding the early oxidation process It can obtain in some detailed information such as bond length between oxygen and metal atoms, diffusivity, electron density adsorption energy and so on. Several computational studies have been conducted to characterize atomistic structure and oxidation process of Ni and Ni-base alloys. [15-20].

1.2. Goal and approach

The main goal of this thesis is to understand the effect of structural changes at oxide layer in nickel based alloy from computational approaches and X-ray experiments. The first principles and MD simulation have been applied to investigate changes in the behavior of oxygen atoms due to the alloying elements during the early stage oxidation process. For supporting the computational method and to

investigate the atomistic structure of M/O interface, X-ray reflectivity and high resolution X-ray diffraction was also performed. The figure 1-4 illustrates the approaches and goal to investigate the oxidation process in nickel based alloy at simulated environments.

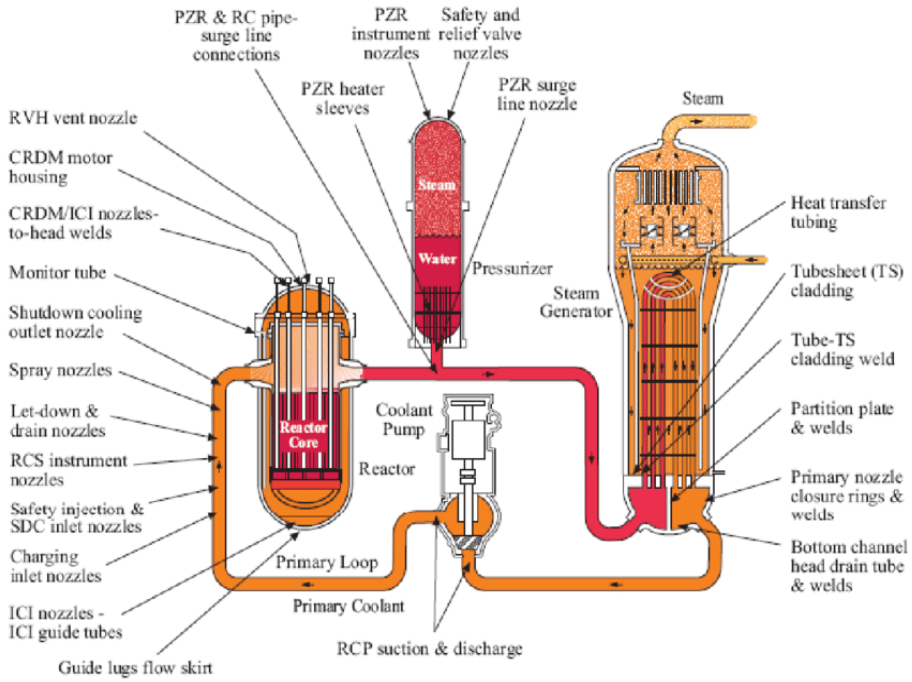

Figure 1-1 The applications of nickel based alloy in pressurized water reactor primary system [2]

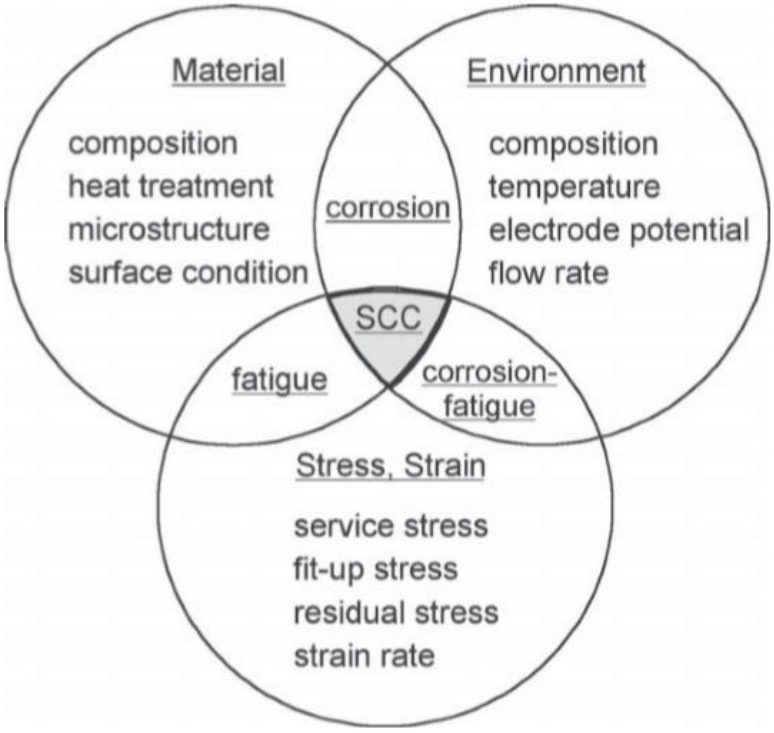

Figure 1-2 Factors affecting stress corrosion cracking [4]

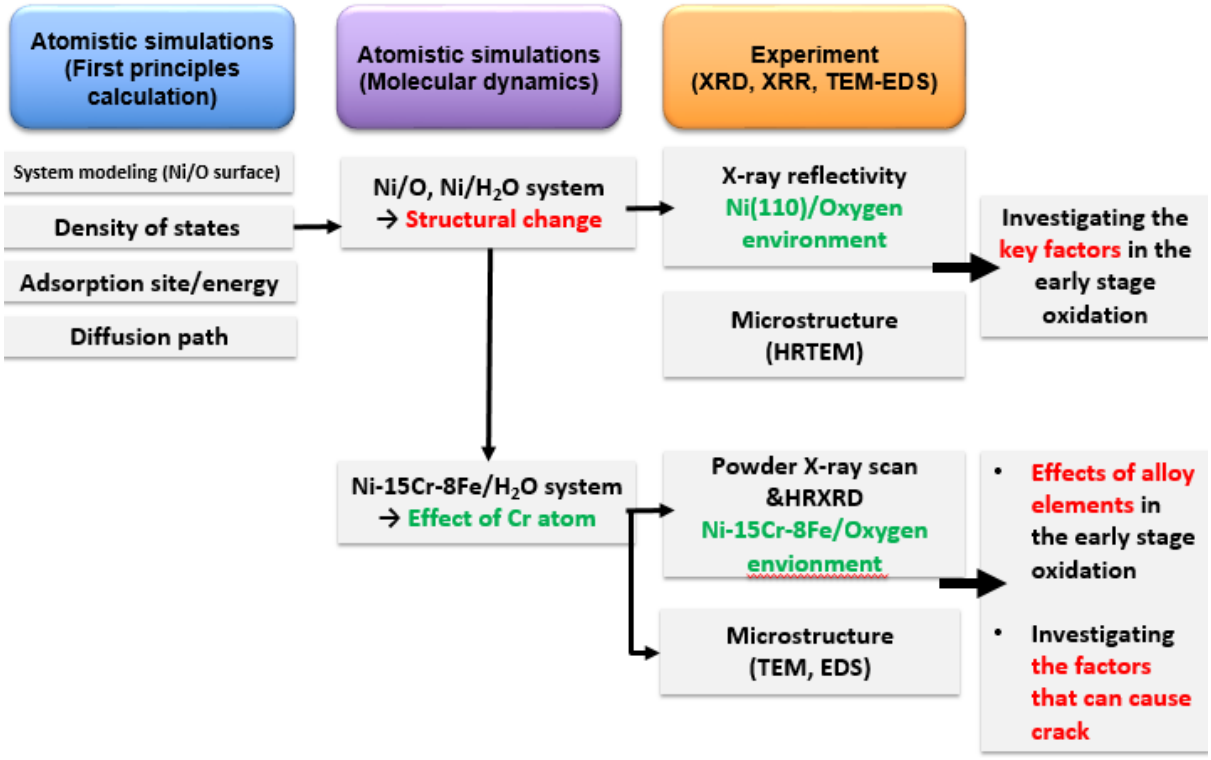

Figure 1-3 A diagram of approaches of this thesis

2. Basic theory and literature study

2.1. Primary Water Stress Corrosion Cracking of Ni-based Alloys

2.1.1. Historical background

The steam generators in early pressurized water reactors were made of austenitic stainless steel, not alloy 600. However, it was found to be vulnerable to stress corrosion cracks caused by chloride. The alloy 600 compensates for these shortcomings and has been used a lot due to its good corrosion resistance than austenitic stainless steel and low corrosion product release rates. However, stress corrosion cracks in the primary water environment for the alloy 600 were identified by Coriou et al. in 1959 [21] and have been found in the alloy 600 for last few decades, causing problems with the integrity of plant structural materials. Figure 2-1 The chronological chart of findings of significant nickel based alloy cracking in nuclear steam supply system plants [22].

SCC is a very complex phenomenon caused by the interaction of metallurgical, mechanical and electrochemical variables. Several mechanisms have been proposed for the PWSCC model since it was discovered by Coriou et al. that SCC can occur in alloy 600. Among the PWSCC models studied by many researchers, the two models presented below are likely related to the PWSCC process.

2.1.2. Hydrogen based mechanism

The main environmental factors affecting PWSCC are temperature, hydrogen concentration and pH value. In addition, the oxidation structure was found to be affected by the concentration of DH. Due to the different properties of the oxide, the sensitivity to PWSCC varies depending on the DH concentration. From previous studies, the initiation time and growth rate of PWSCC are known to be affected by the concentration of hydrogen dissolved in primary water. The thickness of the oxide layer of nickel-based alloys shows that the hydrogen concentration changes as it changes as shown in the Figure 2-2, 2-3 and 2-4 [23-25]. This may mean that substrate is not sufficiently protected by the oxide layer, which makes the material vulnerable to SCC compared to the dense oxide layer.

2.1.3. Internal oxidation mechanism

The internal oxidation mechanism is a specific form of corrosion in which the oxidation of the main elements of an alloy occurs relatively little. Therefore, the less reactive alloy elements are oxidized within the material. Oxidation damages the surface of the metal, resulting in grain boundary oxidation and formed oxide layer can be brittle, resulting in cracks, and then the crack propagation is occurred by

periodic oxidizes the grain boundaries and produces brittle oxide layers. The representation of the internal oxidation mechanism as shown in figure 2.5 [26,53-56].

The internal oxidation model is currently considered one of the leading mechanisms to account for the SCC generation of alloy 600 in PWR. This is because oxygen has been identified at the grain boundary that exists under the metal-oxide layer interface of alloy 600 [27, 28]. In addition, the structure of the crack tip of IGSCC in alloy 600 is found to be similar to the internal oxidation model. As shown in the figure 2-6 [29], NiO structure oxide is present along the crack, and Cr_2O_3 is found to be present in the crack tip, which is made of chromium oxidation [30].

Finally, the internal oxidation model is the only mechanism that can explain both initiation and propagation processes of cracks. We show that the duration of time until cracks calculated through equations 2.1 and 2.2 are generated and detectable cracks are observed is consistent with the results obtained experimentally [57].

$$t_i \propto {a_{cr}}^2 \tag{2.1}$$

$$t_i \propto (K_{ISCC}/\sigma)^4 \tag{2.2}$$

t_i = Crack initiation time

a_{cr} = Critical depth

$K_{ISCC} = \sigma\sqrt{\pi \cdot a_{cr}}$ = Critical stress intensity factor

σ = Applied stress

As such, internal oxidation models account for most of the major thermodynamics and motor behaviors observed experimentally, but there are several unexplained drawbacks, and studies are being conducted to compensate for them.

2.2. Computational Science Methodology

The first principles calculation is called first principles or ab-initio calculation. It is done using the basic principles of quantum mechanics without relying on any experimental or empirical facts. Based on the basic principles of electron-to-nuclear interaction and electron-to-electron interaction without using any empirical or experimental facts, the first method of computing is to solve Schrodinger's

equation to obtain various properties of matter: structural, thermodynamic, electromagnetic, and optical. Several methods have been developed, but the structure and electronic state of solid oxides are often used by DFT (Density Functional Theory).

Density function theory is a computational quantum mechanics modeling method used to investigate the electronic structure of atoms or molecules in fields such as physics, chemistry, and material science. Using this theory, you can represent the properties of a poly electronic system through a function. Nevertheless, there are disadvantages in calculating intermolecular interactions and transition states, which have led to the recent use of molecular dynamics in parallel.

Molecular dynamics is a computer simulation method that analyzes the physical motion of atoms and molecules. Atoms and molecules can be calculated through interaction for a certain amount of time. This calculation is determined by numerically interpreting Newton's equations of motion for interacting particle systems, where the forces between particles are usually calculated through interatomic potentials or molecular mechanics force fields.

In this thesis, we used the reactive force field potential among interactive potentials. ReaxFF potential is suitable for computing bonds between atoms using the length of bonds and the ordered relationship. It can be used in covalent bonds, metal and ionic materials, and the interactions between these materials can also be calculated.

2.3. X-ray experimental Methodology

The three dimensional structure of the sample can be unambiguously determined by using single crystal x-ray diffraction. Many minerals such as diamond and salt, organic molecules appear as small crystals. In these crystals, atoms, ions or molecules are tidied in highly ordered structure, making crystal structure that extends in all three dimensions. This crystal lattice acts as a diffraction grating for X-rays. X-rays are high-energy light with a repeating period called a wavelength or lambda. Since the wavelength of X-ray light is similar to the distance between atoms in a crystal, X-ray diffraction can be used to determine the distance between atoms in the crystal. When an X-ray encounters an atom, its energy is absorbed by the atom's electrons. Electrons occupy special energy states around an atom. Since the absorbed energy is not large enough to release the electron, the energy must be re-emitted in the build of X-ray which have other wavelength, with the same energy as the original. This phenomenon is elastic scattering.

In a crystal, the repeating arrangement of atoms, ions or molecules forms a lattice with well-defined repeating distances. When planes in these lattices are exposed to X-ray beam, X-rays are scattered by this general arrangement. The strong amplification of the emitted signal occurs at certain angles where

the scattered waves constructively interfere. This phenomenon is called diffraction. The XRD method can analyze the structure of crystal in atomic units by measuring these diffracted x-rays.

The tools that can investigate the atomic-scale structure of a surface in ultra-vacuum conditions include useful methods such as electron, ion, and X-ray diffraction. However, most of these surface techniques have the disadvantage that they cannot be applied to surfaces in contact with water from the perspective of material-water interface research. The study of metal and water interfaces is one of the most important factors in terms of metal corrosion because the beginning of oxidation reactions takes place in metal and water surfaces. Therefore, many studies have been conducted using X-ray reflectivity measurements to address these shortcomings, and the underlying theory has been summarized by P. Fenter [31].

The basic principle of X-ray reflectivity is to directly reflect the beam on the surface and measure the intensity of the reflected X-ray in a particular direction. X-rays are mainly scattered by electrons, causing interference. Depending on the surface characteristics, constructive interference or destructive interference occurs, which follows Bragg's law in Equations 2.3.

$$n\lambda = 2d\sin\theta \tag{2.3}$$

n = Diffraction order

λ = Wave length

d = Bragg's plane spacing

θ = Incident angle of X-ray

In equation 2.3, the conditions for constructive interference require the path difference between the two wavelengths to be integer multiple of the wavelengths. The Instead of describing the interference conditions in terms of angles, you can represent them as momentum transfer vector Q, a vector with magnitude and orientation in the reciprocal space. Applying this to Equations 2.3 can be represented by Equations 2.4 and 2.5. Figure 2-7 illustrates the bragg scattering geometry.

$$\boldsymbol{Q} = \boldsymbol{K_f} - \boldsymbol{K_i} = k(\boldsymbol{u_f} - \boldsymbol{u_i}) \tag{2.4}$$

$$Q = |\boldsymbol{Q}| = \frac{4\pi}{\lambda}\sin\theta \tag{2.5}$$

u_f = Unit vector of reflected beam direction

u_i = Unit vector of incident beam direction

In equation 2.4 and 2.5, u_f and u_i with having vector $\mathbf{K} = \frac{2\pi}{\lambda}$ and $\boldsymbol{Q}$ has units of inverse angstroms. The scattered X-ray intensity measured is calculated by summing the scattering amplitudes, ε_j, for each atom, j. In the ideal sample, the sum of all the scattering amplitudes is called the structural factor F, and the intensity of the reflected beam is proportional to the square of F, so the following equation can be obtained:

$$I \propto \left|\sum \varepsilon_j\right|^2 = |F|^2 \tag{2.5}$$

For the actual sample, the equation for a lattice with N layers with a regular separation of atomic layer c and having scattering strength f_0 is defined in equation 2.6.

$$\begin{aligned} F &= f_0\{1 + \exp(-iQc) + \exp(-i2Qc) + \cdots + \exp[-i(N-1)Qc]\} \\ &= f_0 \exp\left(-\frac{i(N-1)Qc}{2}\right)\left[\frac{\sin\left(\frac{NQc}{2}\right)}{\sin\left(\frac{Qc}{2}\right)}\right] \end{aligned} \tag{2.6}$$

Using this relationship, we calculate that the scattering intensity is

$$I \propto |F|^2 = |f_0|^2\left[\frac{\sin\left(\frac{NQc}{2}\right)}{\sin\left(\frac{Qc}{2}\right)}\right] \tag{2.7}$$

In figure 2-8 shows the scattered X-ray intensity of a sample with different atomic layers N. When N=1, the intensity of scoped x-ray results are shown to be flat free of interference. N value increases, strength and sharpness increase around the Bragg peak as shown in Fig 2-8 [31]. In the semi-infinite lattice cases, which do not interfere with the scattered X-rays at the top interface, do not appear to oscillate, unlike previous results. The linear attenuation of X-rays over a distance, x, follows the form $\exp(\frac{-x}{\Lambda})$, where Λ is the linear attenuation length and η is the typical per-layer attenuation factor.

$$F_{CTR} = f_0\{1 + \eta\exp(-iQc) + \eta^2\exp(-i2Qc) + \cdots + \eta^{N-1}\exp[-i(N-1)Qc]\}$$

$$= f_0 \frac{1}{1-e^{-iQc}} \qquad (2.8)$$

In the equation 2.8, when N value is increased and the value of η converges to zero, can derive equation 2.9.

$$I_{CTR} \propto |F|^2 = \frac{|f_0|}{4sin^2(\frac{Qc}{2})}^2 \qquad (2.9)$$

From XRR measurement, the single crystal nickel single crystal sample were used for investigating the early stage oxidation of water/oxide interface.

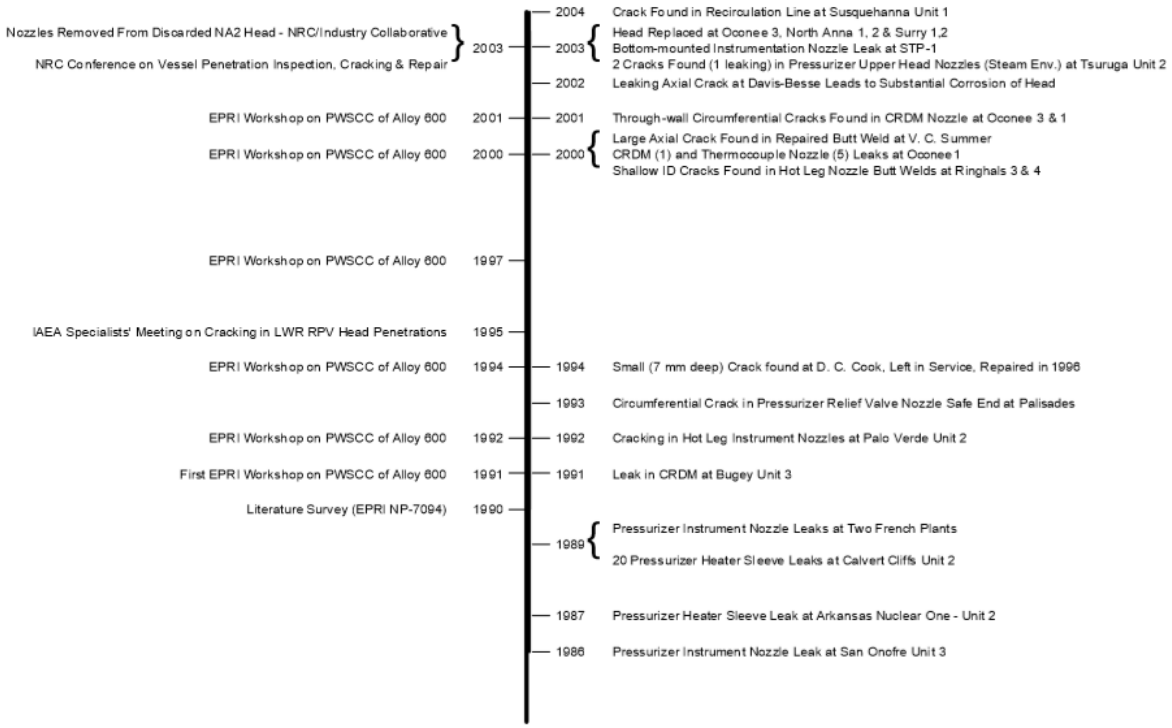

Figure 2-1 The chronological chart of findings of significant nickel based alloy cracking in nuclear steam supply system plants [22]

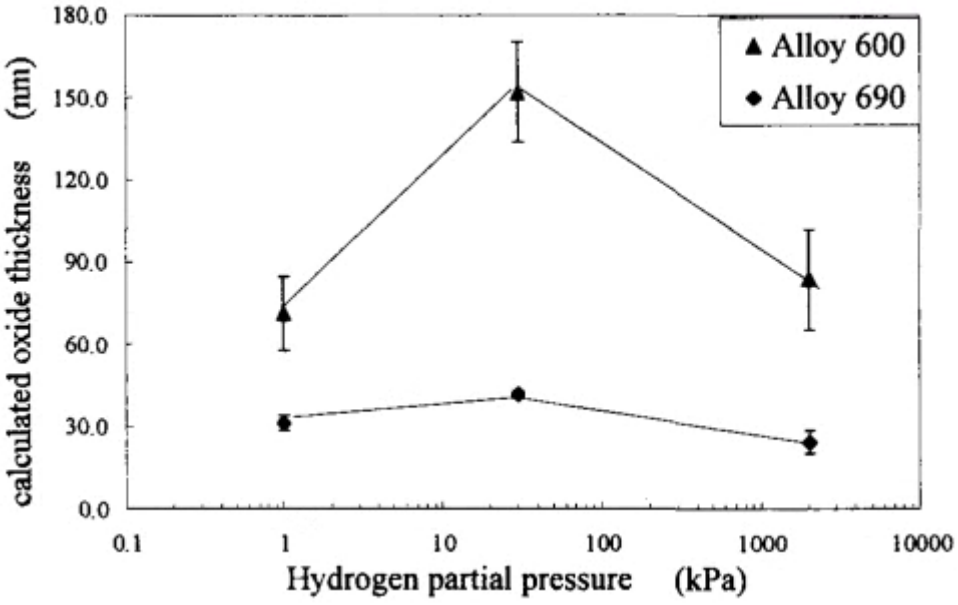

Figure 2-2 The calculation of the thickness of oxide layer from the weight measurement [23]

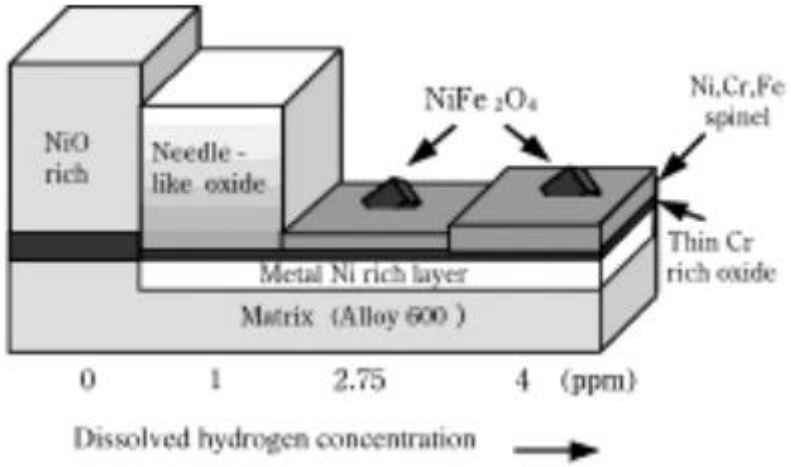

Figure 2-3 Schematic diagram of the oxide layers with various DH conditions [24]

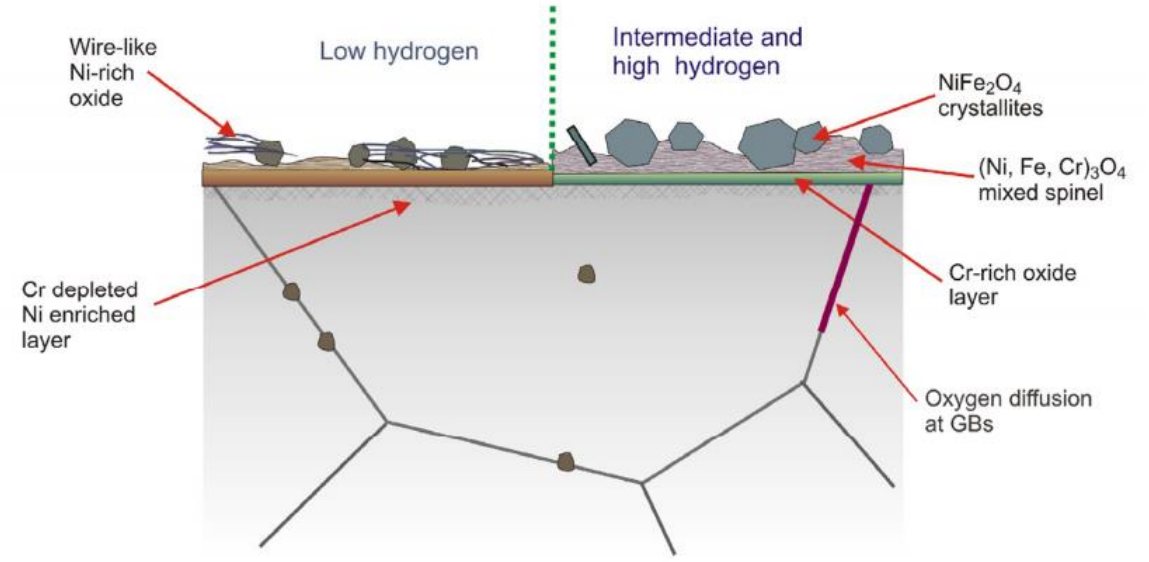

Figure 2-4 Schematic diagram of the interface region (left : lower DH level, right : intermediate and high DH level) [25]

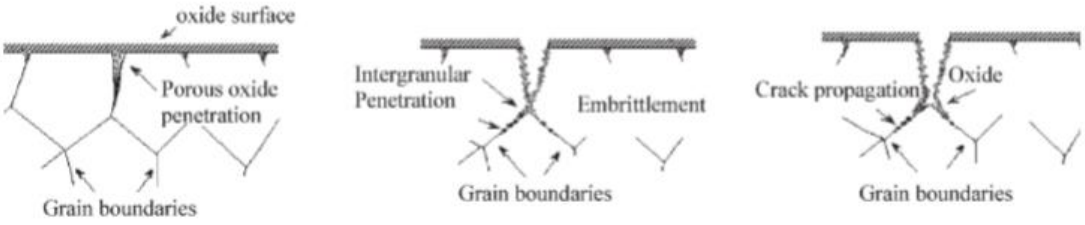

Figure 2-5 Schematic diagram of the I/O mechanism [26]

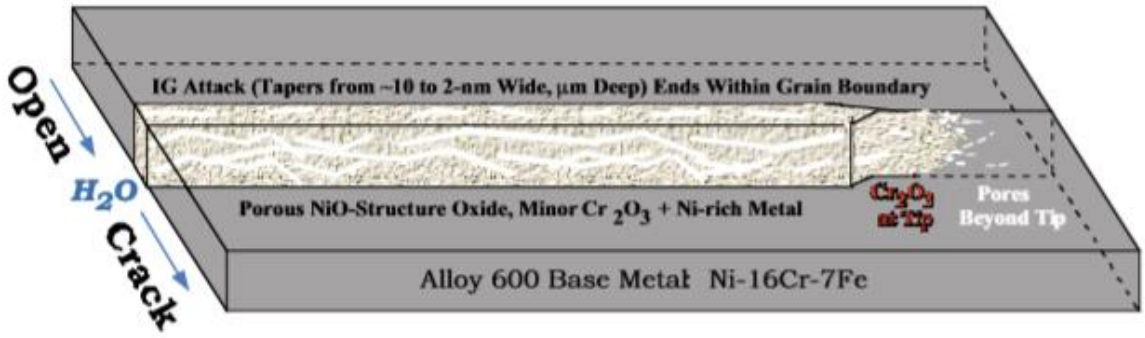

Figure 2-6 The internal oxidation schematic representation [29]

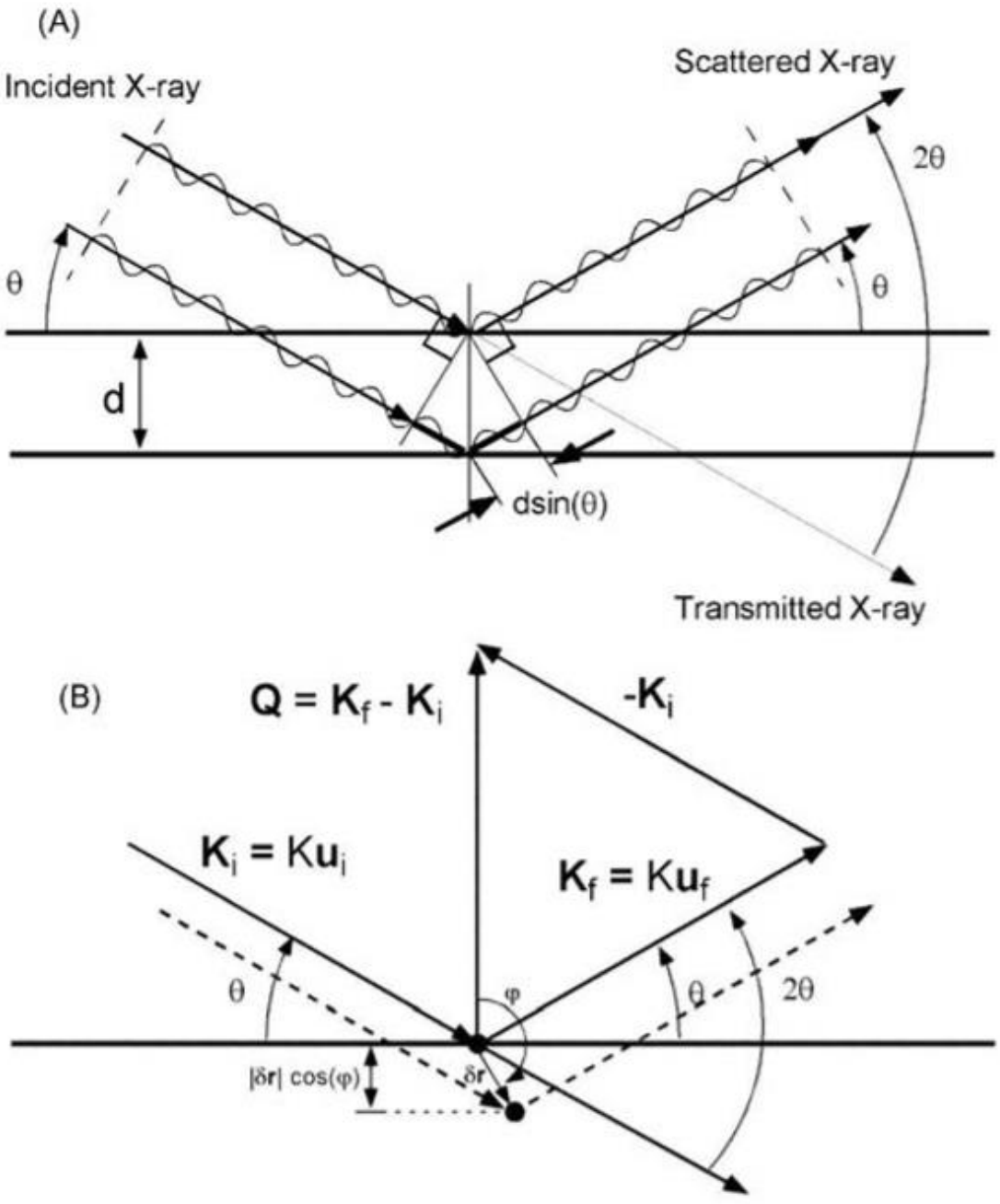

Figure 2-7 The bragg scattering geometry (A) X-ray scattering from two parallel layer (B) describe in terms of vector Q(momentum transfer vector) [31]

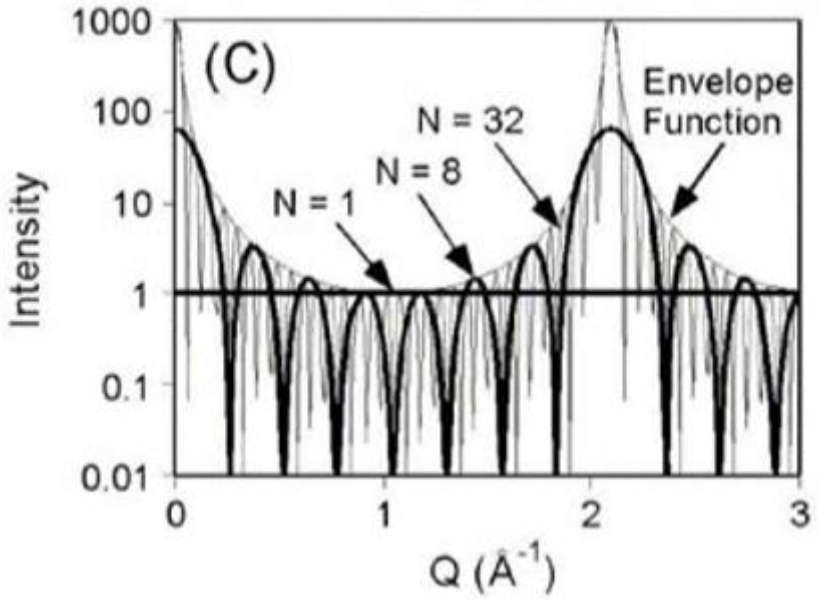

Figure 2-8 The scattered X-ray intensity of a sample with different atomic layer N [31]

3. Methods and materials

3.1. First principles calculation

In this thesis, ab-initio calculations were used as a computational chemistry method based on quantum chemistry. First, in order to calculate the transition state of oxygen diffusion and density of state, ab-initio calculation was performed using the generalized gradient approximation(GGA) and the exchange correlational energy was described using the Perdew and Wang 91 functional(PW91) by the CASTEP module of the Material Studio package. This methodology uses improved for lattice constants, crystal structures and metal surface energy because using conventional local density approximations, it appears to be less accurate in systems where large amounts of charges move [32].

The Ni(110), Ni(100) and Ni (111) surfaces were modeled four layer because interaction of oxygen and nickel substrate were expected from first to fourth layer [33]. Calculations for the surfaces were performed on a 3x3x1 k-point mesh. The convergence tolerance and self-consistent field tolerances were set to 1.0e-6 and 2.0e-6, respectively Figures 3-1 and 3-2 illustrate a Ni(1 1 1) surface after geometry optimization.

In order to calculate the transition state of oxygen diffusion, diffusion of one oxygen atom and of oxygen molecule were considered. In the case of one oxygen atom, the oxygen diffuse from a fcc hollow site (reactant) to a hcp hollow site(product) as shown in Fig 3-3 In the case of oxygen molecule, oxygen molecule diffuse from a fcc-hcp site to a hcp-fcc site as shown in Fig 3-4.

To investigate the adsorption site/energy calculation and the role of diffusion path, we calculated each adsorption site and the diffusion path existing in the Fcc structure as shown in Figure 3-5 and the information of the different adsorption locations is shown in Figure 3-6 ~ 3-8. Through this, when the early stage oxidation process occurred on the nickel surface, we performed an analysis of the important parameters that influenced the oxidation process.

3.2. Ni/O & Ni/H_2O system using Molecular dynamics

To investigate the early stage oxidation of Ni (100), (110), (111) in atomic scale, molecular dynamic calculation was conducted with Large-scale Atomic/ Molecular Massively Parallel Simulator (LAMMPS). LAMMPS is a classical molecular dynamics simulation code designed to be operated efficiently on parallel computers. Many researchers have begun to focus on atomistic modeling to evaluate the interfacial phenomena between materials and water by using LAMMPS. In this study, ReaxFF potentials are used to investigate the early stage oxidation in the Ni/O system modeling.

The molecular dynamics calculations were performed using ReaxFF potential. In the field of corrosion, the developments in ReaxFF potentials originally developed to study the hydrocarbon and the catalytic properties of organic compounds have enabled the investigation of metal and water reactivity. Analysis of trajectories from molecular dynamics with ReaxFF(reactive force field) potential are able to show complex initiation chemistry for the nickel oxidation process.

The ReaxFF potentials have been specifically designed to describe the dissociation, transition and formation of chemical reaction while molecular dynamics simulation with precision to quantum chemical study.

And also it considers the non-bonded interactions between atoms by using coulomb force and van der Walls term. In ReaxFF, the system energy expression is divided into several terms as shown in equation 3.1.

$$E_{total} = E_{bond} + E_{tors} + E_{coulomb} + E_{vdW} + E_{h-bond} \quad (3.1)$$

All calculations were modeled by the periodical array. The periodical array was cut in <0 0 1> direction to create the Ni (100), (110), (111) surface. To simulate detailed initial oxidation process mechanism of Ni/O & Ni/H_2O system, 864 oxygen atoms and 12480 nickel atoms were positioned in a cubic periodic box with 84.48 × 42.24 × 84.48 Å. The vacuum slab was set over the nickel surface with lattice parameter is 3.52 Å. For the reactive force field simulations, the system was performed energy minimization step first and constant volume–temperature (NVT) reactive simulations were performed at temperature of 550 K for a 10 nanoseconds. In each calculation, the lattice relaxation time was set as 5 ns. All oxygen atoms are randomly distributed over the nickel surface as shown in Fig. 3-9 and 3-10. The upper section of nickel substrate was divided into three sublayers in order to calculate radial distribution function (RDF) and lower substrate was fixed because nickel atoms that located in the substrate are not affected by oxygen atoms.

3.3. Ni-15Cr-8Fe/H_2O system using Molecular dynamics

To investigate the effect of alloying elements and the factors that can cause crack initiation in the early stage oxidation of Ni-15Cr-8Fe/H_2O in atomic scale, molecular dynamic calculation was conducted with LAMMPS. The molecular dynamics calculations were performed using ReaxFF potential [34].

All calculations were modeled by the periodical array. The periodical array was cut in <0 0 1> direction to create the Ni-15Cr-8Fe surface. To simulate detailed early stage oxidation process mechanism of Ni-15Cr-8Fe/H_2O system, 864 oxygen atoms, 1872 chromium atom, 998 iron atom and 12480 nickel atoms were positioned in a cubic periodic box with 84.48 × 42.24 × 84.48 Å. The vacuum slab was set over the nickel surface with lattice parameter is 3.52 Å. For the reactive simulations, the system was minimized first and constant volume–temperature reactive simulations conducted at temperature of 550 K for a 40 nanoseconds. In each calculation, the lattice relaxation time was set as 5 ns. All water molecules are randomly distributed over the nickel surface as shown in Fig. 3-11.

3.4. X-ray experiments

3.4.1. X-ray reflectivity of Ni single crystal

In this thesis, we employed an integrated approach using high-resolution X-ray reflectivity (HRXR) [35-36] to obtain a comprehensive understanding of the early stages of oxidation on Ni(110).

HRXR measurements were performed to probe the interface structure between the nickel oxide and the Ni(110) single crystal substrate with atomic resolution. The detail of the specimen is shown in Table 3-1 and Figure 3-12.

The pre-treatment process was performed in the order of mechanical grinding – Ar Sputtering – Annealing – formation of passivity film, among which Ar-sputtering and Annealing processes were performed four times. In the mechanical grinding phase, the grinding phase using SiC paper and polishing phase using Diamond Suspension solution and Alumina Suspension solution were performed as in the normal metal specimen treatment. In the process of performing, the pressure applied to minimize residual stress caused by surface friction was minimized and each step was performed for more than 30 minutes. Single-crystal specimen with completed grinding of electricity is loaded into a chamber with a vacuum degree of less than 10^{-10} torr. The chamber is equipped with argon ion etching equipment, RHEED guns and screens, and leak valves for oxygen injection. The surface was etched using argon ions with an energy of 0.5 kV and 10 mA in the loaded specimen, and the process was carried out for 10 minutes. The single crystal specimen was heat treated in the ultra-high vacuum chamber. The process is intended to relieve residual stress on the surface that may occur during argon ion sputtering. Using the correlation expression of the sample surface temperature-heater temperature measured before the experiment, the heater was heated to that temperature by measuring the heater temperature at which the surface temperature could reach 700℃. After the surface temperature reached 700℃, it was maintained for 5 minutes, and the heater heat was then shut down to cool the specimen in

the vacuum until the surface temperature dropped below 40 degrees. Ion etching – heat treatment process was repeated four times in total to improve surface crystallinity. A trace amount of oxygen was injected into the chamber to form a floating film layer on the surface of a single crystal specimen that has completed ion etching and heat treatment. The fractional pressure of oxygen is $4.0 * 10^{-6}$ torr, which is known to grow epitaxial oxide membranes on the surface of nickel and nickel-chrome alloys under the corresponding oxygen fractional pressure conditions.

Surface properties are analyzed through RHEED techniques during the pretreatment process to understand surface changes according to the pretreatment process. The results of the RHEED diffraction pattern analysis according to the pretreatment process in Figure 3-13 show that the more Ar-sputtering and annealing processes, the clearer the RHEED pattern becomes. Furthermore, the surface geometry of the specimen before and after the specimen pre-treatment (after the formation of a floating film) was analyzed through AFM as shown in Figure 3-14.

The prepared specimen analyzed the underlying properties of nanometer-thick antifreeze membranes formed on surfaces via GIXR techniques at the Advanced Photon Source (APS), Argonne National Lab's radiation accelerator facility in the United States. The beamline consists of a 6-Axis Goniometer, a Pilatus 100K Area Detector, and so on, which used x-rays with 18 keV energy conditions in the experiment.

3.4.2. X-ray diffraction of Ni-15Cr-8Fe single crystal

The detail of the specimen are shown in Table 3-2 and the surface pretreatment process was done in the same method as Ni single crystal sample. The Ni-15Cr-8Fe specimen was performed through KIST's Powder x-ray scan and High resolution x-ray diffraction equipment. The equipment consists of two goniometer, copper x-ray source. The goniometer radius is 185 mm, and maximum x-ray power is 18kW(60kV, 300mA).

The experiment was conducted to investigate the initial oxidation process on the metal surface, using handled specimens with the same conditions as the X-ray reflectivity experiment.

Table 3-1 The description of nickel single crystal specimen

Size	Orientation	Composition(wt.%)
2.35mm × 2.05mm × thickness 0.80mm	(110)	Ni
		100

Table 3-2 The description of Ni-15Cr-8Fe single crystal specimen

Size	Composition(wt.%)		
diameter 6.00 × thickness 1.00mm	Ni	Cr	Fe
	Bal.	15	8

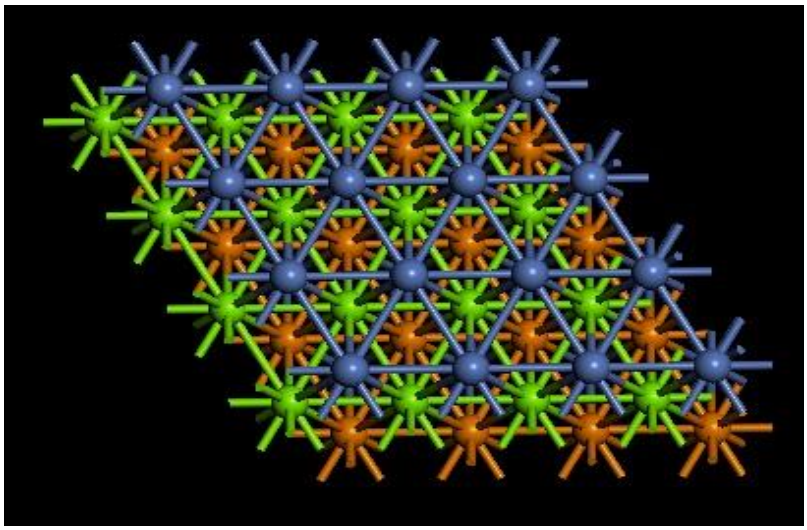

Figure 3-1 Top view of the nickel (111) surface, where the different colors indicate different layers: blue, the 1st layer; green, the 2nd layer; yellow, the 3rd layer

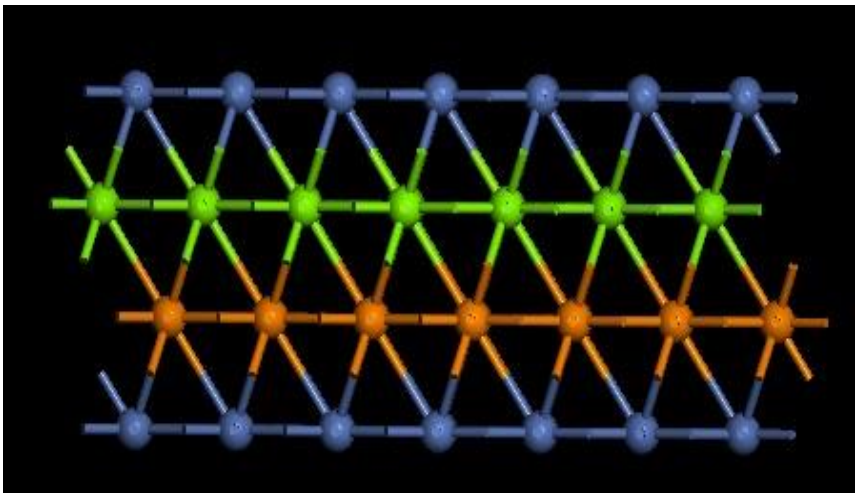

Figure 3-2 Side view of the nickel (111) surface, where the different colors indicate different layers: blue, the 1st layer; green, the 2nd layer; yellow, the 3rd layer

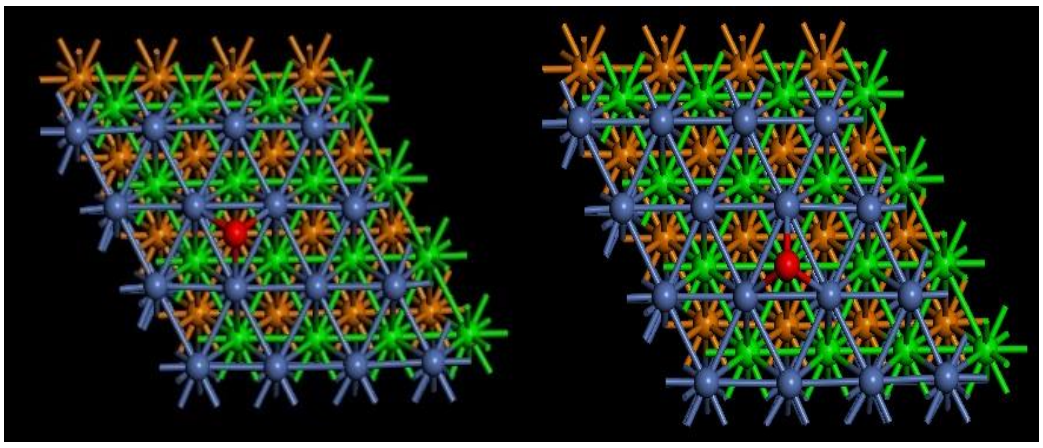

Figure 3-3 Top view of the Ni(1 1 1) surface with one oxygen atom(red) located on hcp(left) and fcc(right) hollow sites

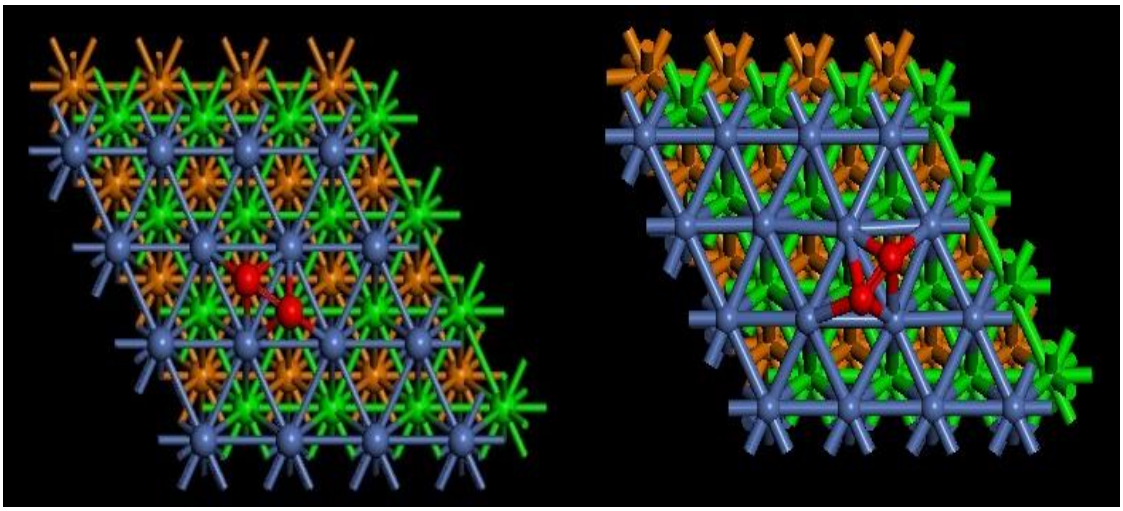

Figure 3-4 Top view of the Ni(1 1 1) surface with two oxygen atom(red) located on hcp and fcc hollow sites

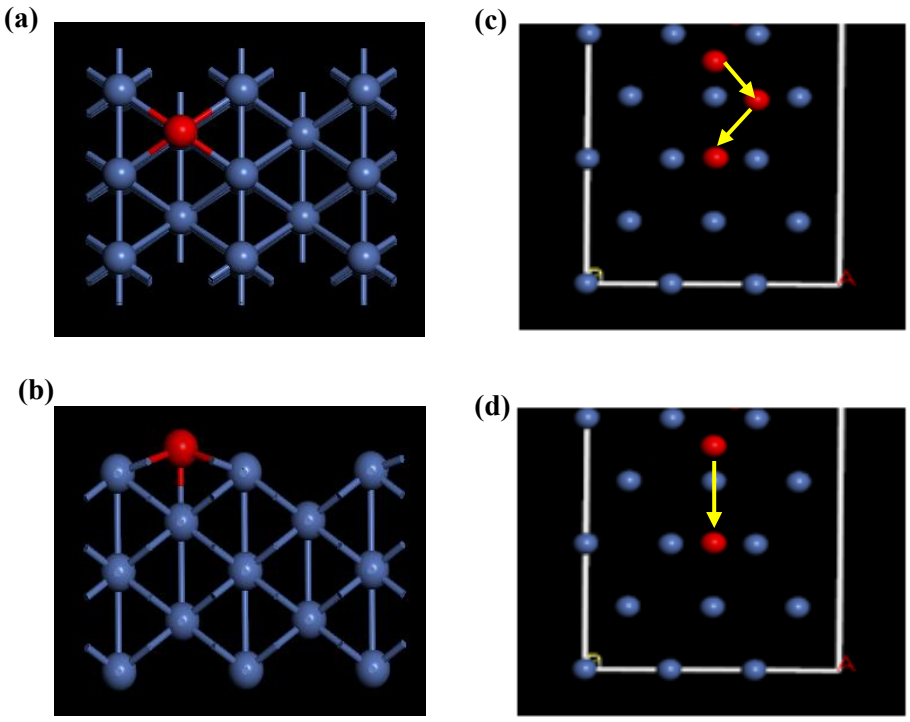

Figure 3-5 (a) Top view of the Ni surface with one oxygen atom(red) located on hcp hollow sites (b) side view of the Ni surface with one oxygen (c) Side view of the Ni substrate with one oxygen atom(O-T-O path) (d) Side view of the Ni substrate with one oxygen atom (O-O path)

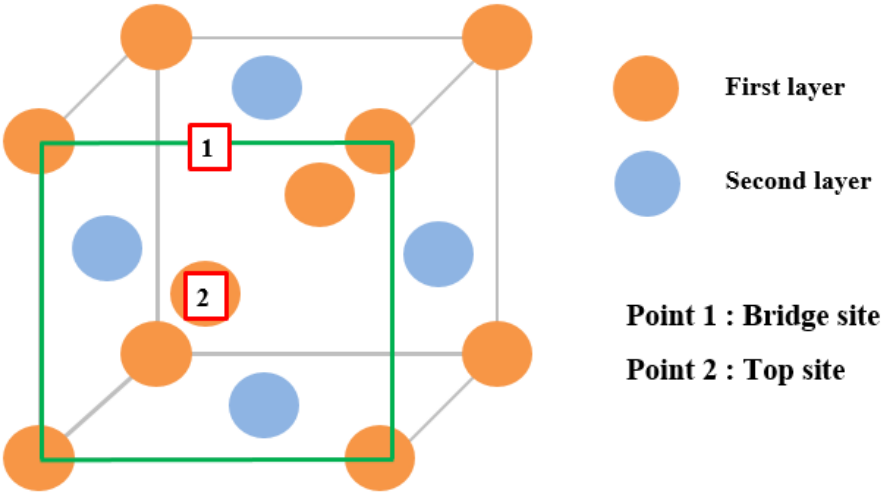

Figure 3-6 The adsorption site on the Ni(100) surface

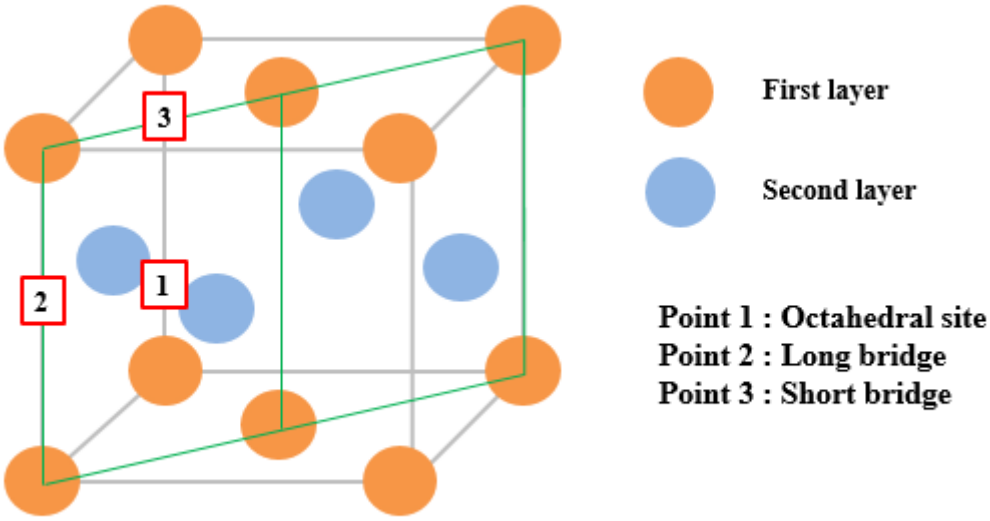

Figure 3-7 The adsorption site on the Ni(110) surface

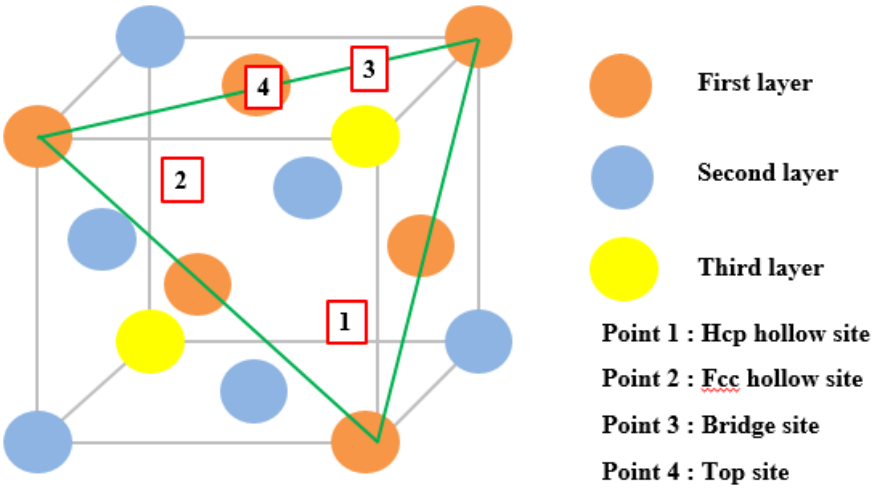

Figure 3-8 The adsorption site on the Ni(111) surface

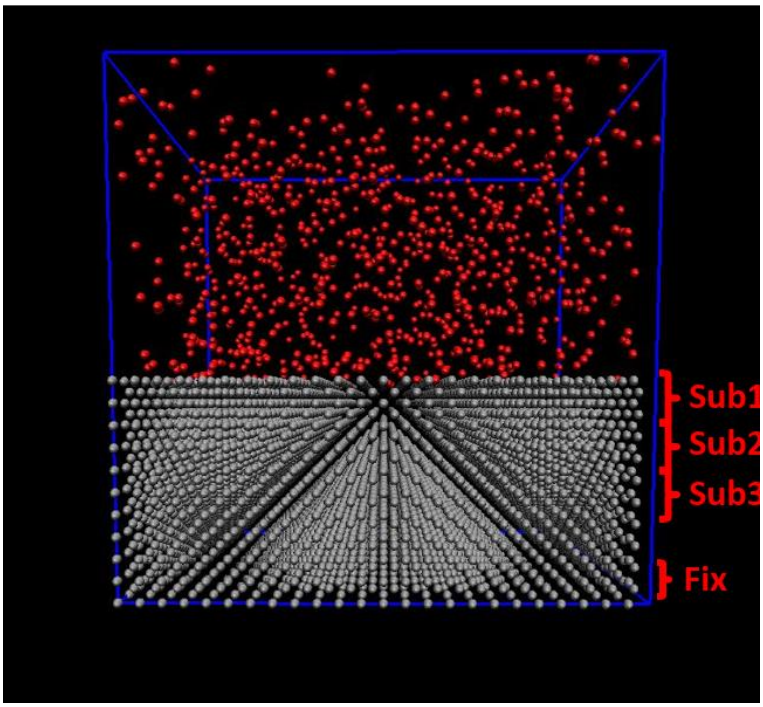

Figure 3-9 Initial state of Ni/O system

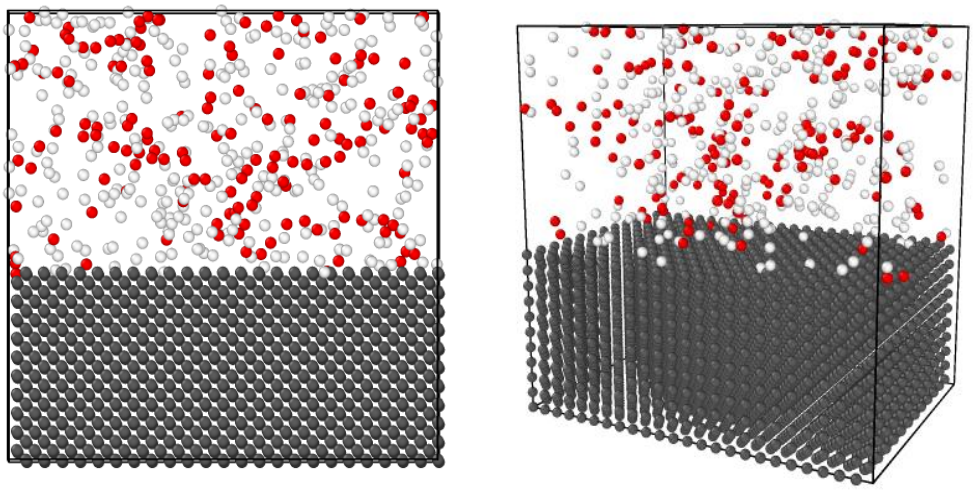

Figure 3-10 Initial state of Ni/H_2O system

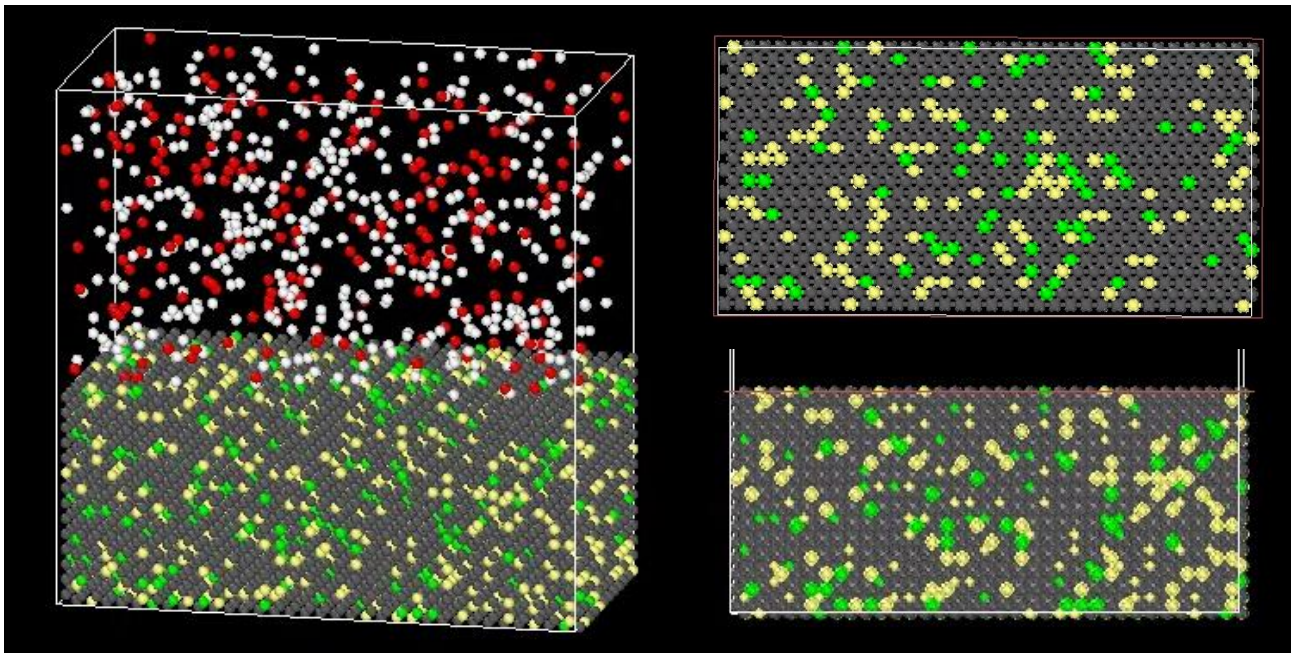

Figure 3-11 Initial state of Ni-15Cr-8Fe/H_2O system (red : oxygen atom, grey: nickel atom, white : hydrogen atom, yellow : chromium atom, green : iron atom)

Figure 3-12 Sample and Sample holder for surface pretreatment

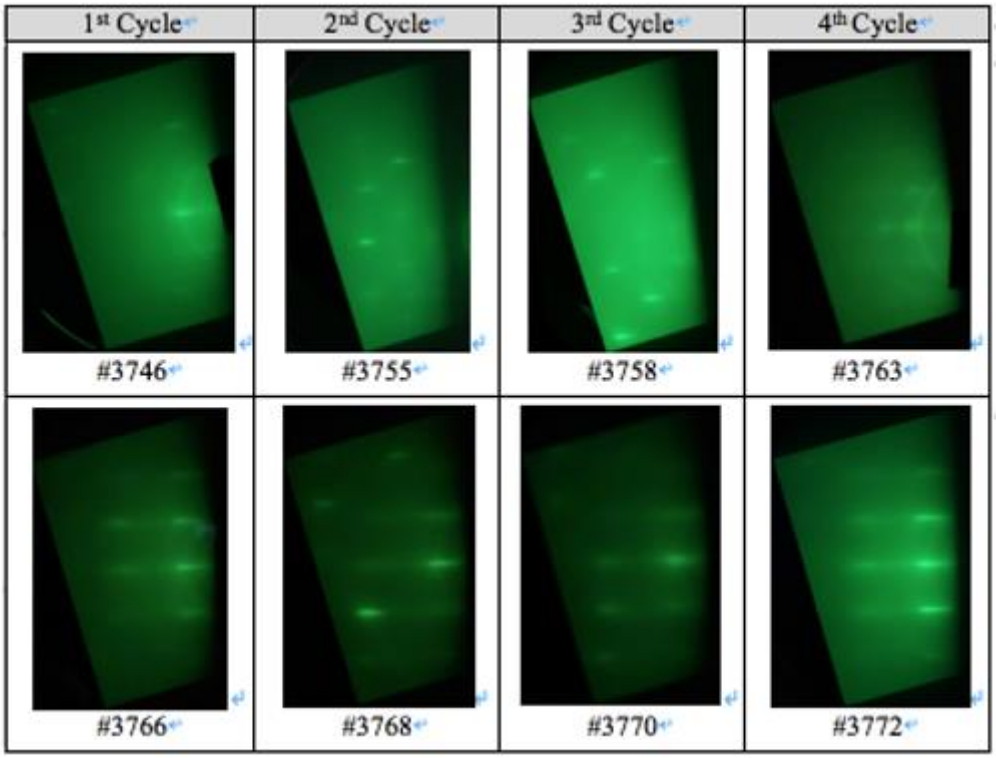

Figure 3-13 Results of RHEED diffraction pattern analysis according to pretreatment process

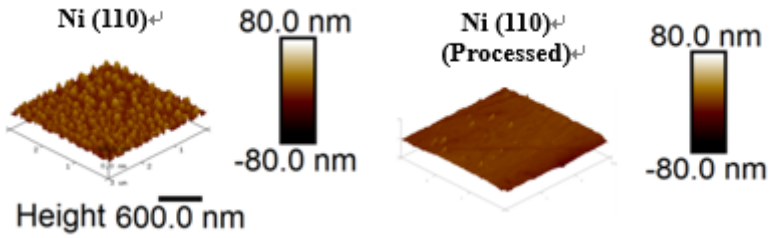

Figure 3-14 Analysis of specimen surface geometry with AFM before and after pretreatment

4. Results

4.1. First principles calculation

4.1.1. Partial density of states

To demonstrate the first-principles calculation result, the density of states(DOS) was calculated to analyze the interaction mechanism between the nickel surface and an oxygen atom. When metal interacts with an atom or molecule, the d orbital of the metal combine with the atom or molecule as shown in Figure 4.1. [37-38]. Additionally, Soft X-ray emission spectroscopy result demonstrated the hybridization between d orbital of nickel and the oxygen p orbital as shown in Figure 4-2 and 4-3 [39]. In the DOS calculation, we observed two peaks for oxygen atoms [40]; one corresponding to the s orbital with energy ranging from –19eV and -18eV and the other corresponding to the p orbital with energy ranging from -6eV and -4eV. Therefore, Ni interacts with oxygen because the DOS of the d orbital of Ni overlaps that of the p orbital of oxygen atom as shown in Figure 4.4.

4.1.2. Adsorption energy

The process of oxygen adsorption to metals is one of the important parts of the initial oxidation process. Adsorption energy calculations were performed to analyze where oxygen is adsorbed to form and grow an oxide layer. As previously described, the nickel surface was constructed using bulk optimization grid parameters. Previous studies have verified that this model is suitable for calculating water adsorption for alloys or pure transition metals [58-60]. The adsorption positions such as hcc hollow site, hcp hollow site and Octahedral site exist on the surface of metals with a face centered cubic structure such as nickel.

Each adsorption site has its own energy value when combined with oxygen on the surface. In order to calculate adsorption energy, water molecules bound to a particular adsorption site were modeled and the energy required to move to a different location was investigated to calculate the relative energy value. This is a useful way to find the most stable adsorption site. A relative comparison of these energy values found that the hcp hollow site and fcc hollow site on the Ni (111) surface were the most stable, followed by the Octahedral site on the Ni (110) surface as shown in Table 4-1. As a result, oxygen can be predicted to be the first adsorption to the Ni (111) surface during the initial oxidation process. In addition, when the oxide layer is produced, there is a possibility that oxygen may spread from the site mentioned above, resulting in the growth of oxide island.

4.1.3. Barrier energy

Previous results demonstrate computationally that oxygen is adsorbed in selectively stable positions during the initial oxidation process. In order for corrosion to occur on the metal and water interfaces, oxygen atoms need to penetrate into the substrate. To determine the behavior of these oxygen, the direction of diffusion of oxygen was calculated after the oxygen was adsorbed to the surface by the derivation of Barrier energy from the Transition state calculation.

The figure 4-5 and 4-6 shows the results of the transition state search calculation. The modeling of reactants and products can be calculated relative values of how much energy is needed to move oxygen. These results show that oxygen needs the most energy when diffusion occurs on the surface of Ni (111), followed by Ni (100) and Ni (110).

4.2. Ni/O & Ni/H_2O system

4.2.1. Structural changes of nickel surface

In figure 4-7, The molecular dynamics results of Ni/O system that deducted by using ReaxFF potential are treated. In this result, when the reaction of oxygen and nickel atoms at the surfaces are occurred, therefore it can be confirmed about Ni substrate was divided into several layer(Sub1 - 3). There are three different structure layers in the nickel substrate.

The first sublayer(Sub1) is nickel oxide amorphous layer which is formed by the direct interaction with oxygen atoms. The interaction of oxygen atoms with nickel in high temperature environments leads to the dissolution of nickel atoms and the diffusion of elements and, oxidation takes place at the surface, therefore, the nickel atom which is located in upper section of substrate is reacted with the oxygen atom and forms nickel oxide amorphous layer. It is due to the vigorous intermolecular interactions which is occurred between oxygen and nickel atoms at the surface. Also, the second sublayer(Sub2) is reacted oxygen atoms layer which permeated through the nickel surface. The second layer losses basic characteristic of nickel substrate by oxygen atom and forms another nickel layer that has different lattice parameter than the existing nickel substrate. However, the sublayer3(Sub3) is maintained as a Ni structure. Because, oxygen atom can not permeate into the sublayer3. The thickness of the oxide layer for each surface is shown in the table 4-2.

The Ni/H_2O calculation results also showed similar results to Ni/O system calculations. The difference from the previous results is, The NiO structure formed on the Ni substrate was similar to trigonal NiO with a direction close to (111) as shown in Figure 4-8. The amorphous and crystalline phases co-exist at the interface, suggesting complex growth processes caused by an intrinsic mismatch

between the rectangular lattice of the Ni(110) surface and the stable hexagonal packing of the NiO(111) epitaxy layer and Adaptive common neighbor analysis was performed for the trajectories of the simulation to assign a structure type to each particle from the coordination information. In addition, this model can be show that structural changes occurred not only on the surface but also inside the substrate. As the oxidation process progressed, Ni (111) form of HCP crystal structure was created inside the nickel as shown in Figure 4-9.

4.2.2. Radial distribution function

To evaluate reaction process of oxygen consumption phenomenon and mechanism, the molecular dynamic simulations were performed with a constant volume. And the RDF was used in order to investigate structure change in nickel substrate. The RDF is a statistical mathematics function that is used to describe a cluster or aggregation of objects. RDF (g(r)) is a local measure of how close the observed distribution is to a uniform one.

As shown in figure 4-10, the RDF is calculated for each sublayer in order to investigate the structural change and the effects of oxygen permeation into nickel substrate. In this result, RDF of sublayer1(blue line) indicates smooth curve. The sublayer1 can't be maintained basic characteristic of nickel substrate and forms amorphous nickel oxide layer. Also, sublayer2(green line) is under the influence of oxygen atom, therefore, a difference in radial distribution is shown.

4.3. Ni-15Cr-8Fe/H_2O system

4.3.1. Oxidation behavior analysis

To investigate, effects of alloying elements in the early stage oxidation and the factors that can cause crack, The Ni-15Cr-8Fe/H_2O system was conducted. In the early stages of oxidation, oxygen atoms can be seen bonded to the surface as a whole. The oxygen atoms that were bound to the surface as a whole have been shown to recombine with dissociation due to their reactions to oxygen or water molecule. This phenomenon has also been investigated to affect metal surfaces. The oxygen atoms adsorbed on the surface cause reactions in the water environment and cause dissociation of metal atoms. These dissociated metal atoms react again on the surface, causing bonding on the surface or reacting with water molecule to remain in the water environment. During the modeling of the oxidation process using molecular dynamics simulation, this phenomenon was repeated and oxidation progressed. As oxidation occurs, oxygen atoms that have been bound to the surface as a whole can be found to form an oxide film near the chromium atom over time as shown in figure 4-12.

The preceding results can be observed more clearly from the results of the trajectory oxygen atom method. At the top side of the surface, oxygen atoms combine with metal atoms present on the surface early in the oxidation process to form an oxide layer. However, it can be seen that the position of the atoms changes as surface atoms repeat binding and decomposition due to the continuous oxidation process. Therefore, oxygen atoms bonded to the Nickel atom move toward the Chromium atom to form an oxide as shown in Figure 4-13.

4.3.2. Analysis of oxide layer

In Ni-15Cr-8Fe systems, chromium atoms can be seen migratory to the surface over time by oxidation. Chromium atoms that migratory to the surface react with oxygen and are found to be oxidized. This phenomenon occurred by adsorbed oxygen atoms which located on the surface diffuse into inside the nickel substrate, such as the results of the first principles calculation. When the oxygen atom spreads inside the nickel substrate, it binds to the surrounding metal atom and causes an oxidation process. As the oxidation process continues, chromium atoms which are relatively more oxygen affinity than the nickel atoms were found to move to the part where oxidation occurred inside the nickel substrate. During the early stage oxidation process, most of them were identified as amorphous layers and can be seen to retain their crystallinity in part as shown in figure 4-14. The amorphous layer was found to be a combination of nickel, chromium, iron and oxygen atoms that could not be defined as a specific crystal structure. It has been shown to exist at random locations in three dimensional lattice structures.

The figure 4-15 shows that chromium atoms migrate to the surface to form an oxide layer. It is analyzed that the oxide layer is approximately 6 Å $\pm$ 0.8 Å thick from the surface. Below the oxide layer, the amount of chromium atoms appears to be decreasing. This phenomenon has also been investigated in TEM analysis. This can be seen in Figure 4-16 and Table 4-3.

4.3.3. X-ray experiments of Ni-15Cr-8Fe/H_2O single crystal sample

In the early stage oxidation process, High resolution X-ray diffraction and Powder X-ray diffraction were used to investigate the reaction of Ni-15Cr-8Fe ternary single crystal sample at metal-water interface. The high resolution X-ray diffraction results in Figure 4-17 show that one peak appears at 76deg. This was identified as a peak indicating the (110) direction that the sample had. The Powder X-ray diffraction results show two peaks differently from the HRXRD results. In addition to 76deg peaks, such as HRXRD, peak was observed at 62deg. The peak observed in 76deg appears to be the peak on the same (110) surface as the specimen, and the peak seen in 62deg appears to be the peak on the amorphous layer as shown in Figure 4-18. The difference in the results of the two X-ray diffraction

experiments is that they are single crystal sample, so the diffraction pattern may not appear well. In addition, there is a possibility that the peak does not appear to distinguish it from the background due to the different energy of X-rays.

Table 4-1 The adsorption energy at each adsorption site

	Adsorption energy(eV)
Octahedral site(Ni(110))	2.21
Long Bridge	2.02
Short Bridge	1.93
Hcp Hollow site(Ni(111))	2.59
Fcc Hollow site (Ni111))	2.48
Bridge site	1.71 – 1.75
Top site	1.51 – 1.59

Table 4-2 The thickness of oxide layer for each surface

	Thickness (Å)
Ni (100)	**7.2±0.5**
Ni (110)	**8.1±1.1**
Ni (111)	**6.4±0.7**

Table 4-3 Chemical composition of 5 different point in Fig. 4-13

Type (w.t.%)		Ni	Cr	Fe	O
Surface	1	70.65	16.23	10.07	3.05
Inner surface	2	73.35	15.72	9.71	1.22
	3	73.35	15.59	9.81	1.25
	4	73.52	15.43	9.79	1.27
Substrate	5	74.12	15.87	9.48	0.54

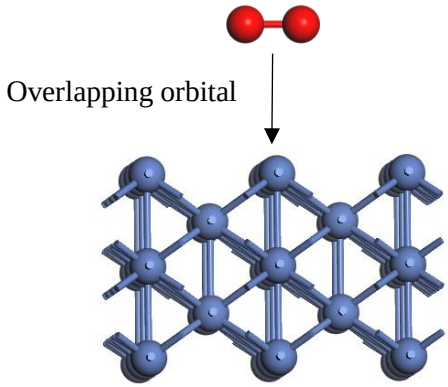

Figure 4-1 Illustration of typical atomic model for the interaction of an atom or a molecule with a metal surface

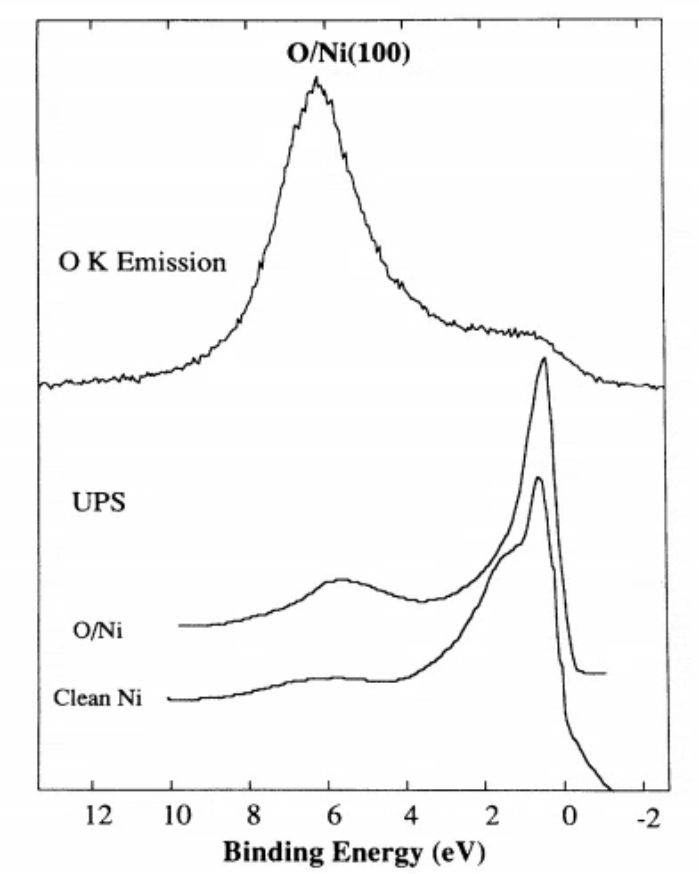

Figure 4-2 The comparison between the SXE and UP spectra from O/Ni(100) [39]

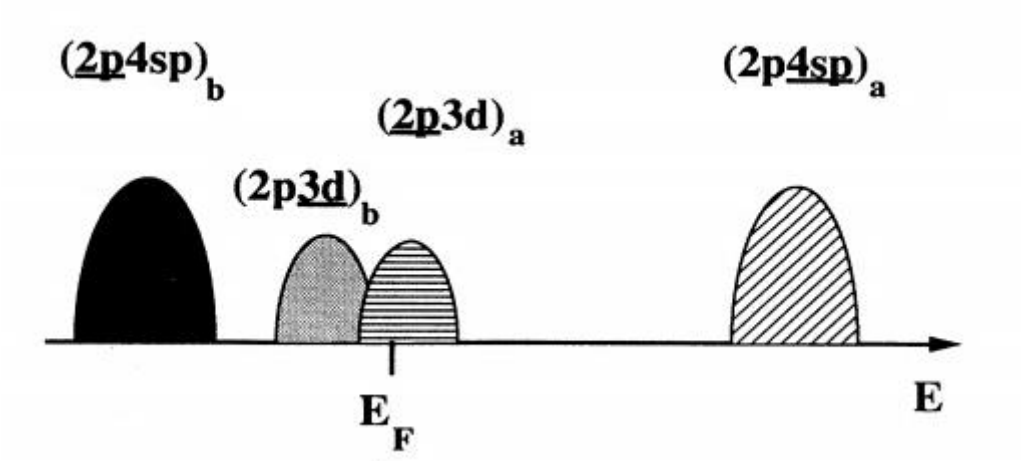

Figure 4-3 Schematic diagram presented a simple model for hybridization between 2*p* of oxygen and 3*d* of nickel [39].

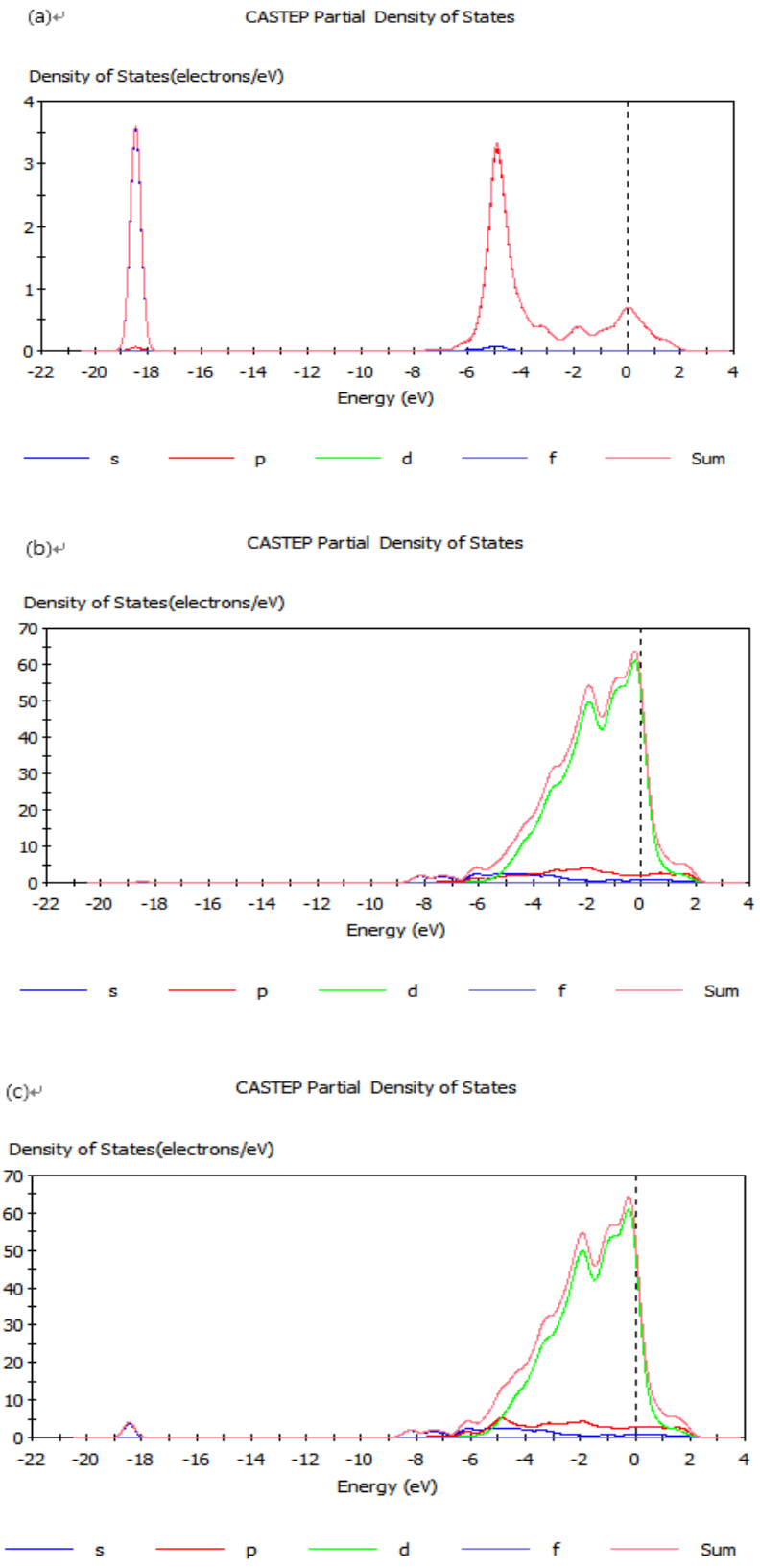

Figure 4-4 Partial density of states for (a) oxygen, (b) a pure Ni surface, and (c) Ni-O system

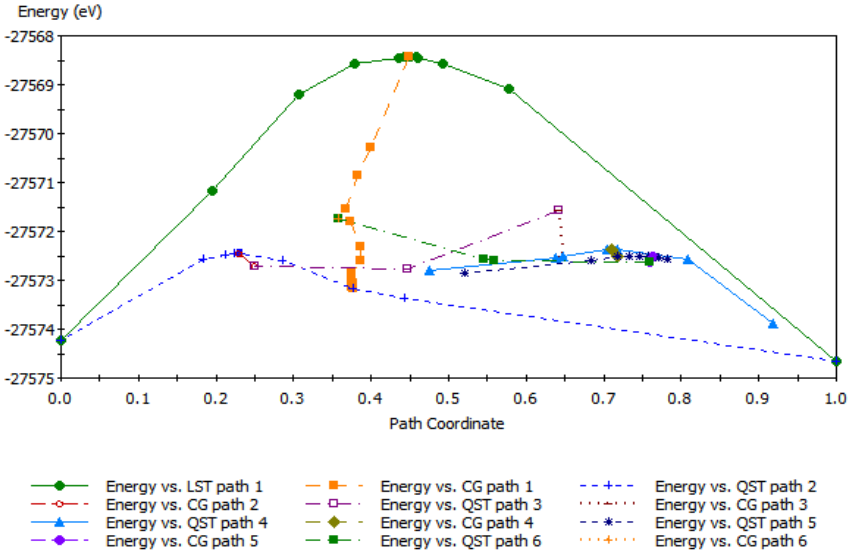

Figure 4-5 Transition state search results for the oxidation Ni surface

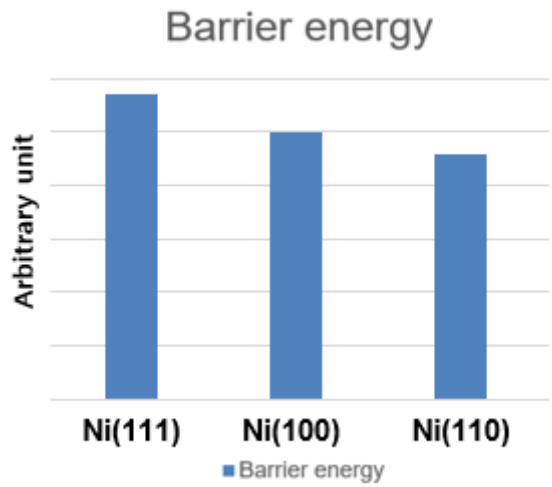

Figure 4-6 Barrier energy of the oxygen diffusion in the NI surface

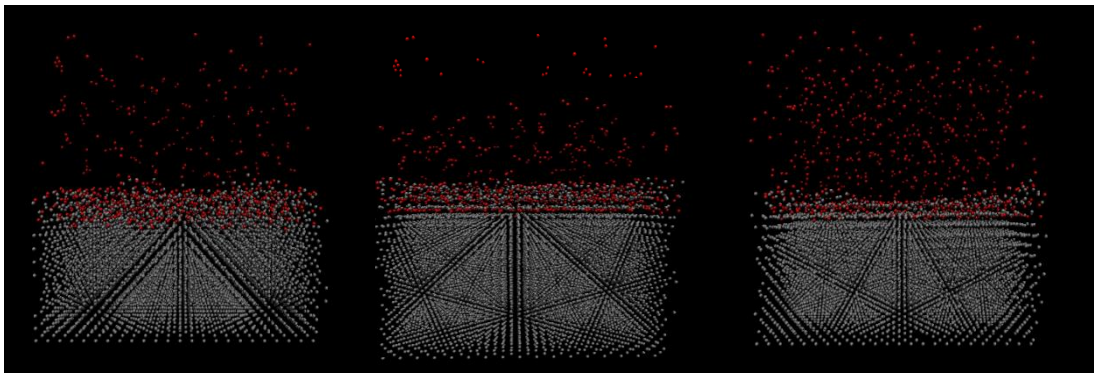

(a) **(b)** **(c)**

Figure 4-7 The illustration of atomic structure model (final state) for interaction of nickel and oxygen on nickel (a) Ni (110) (b) Ni (100) (c) Ni (111) surface

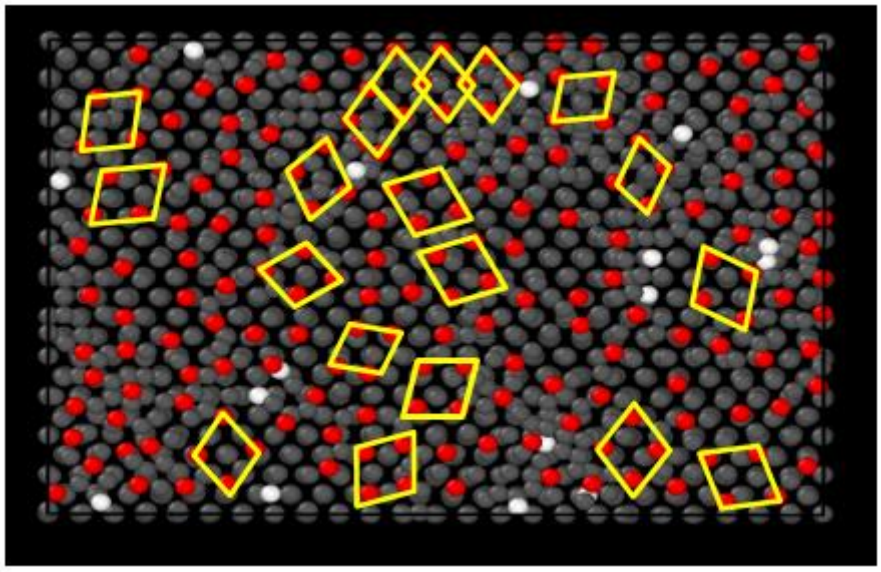

Figure 4-8 Surface structure aspects of Ni/H_2O system

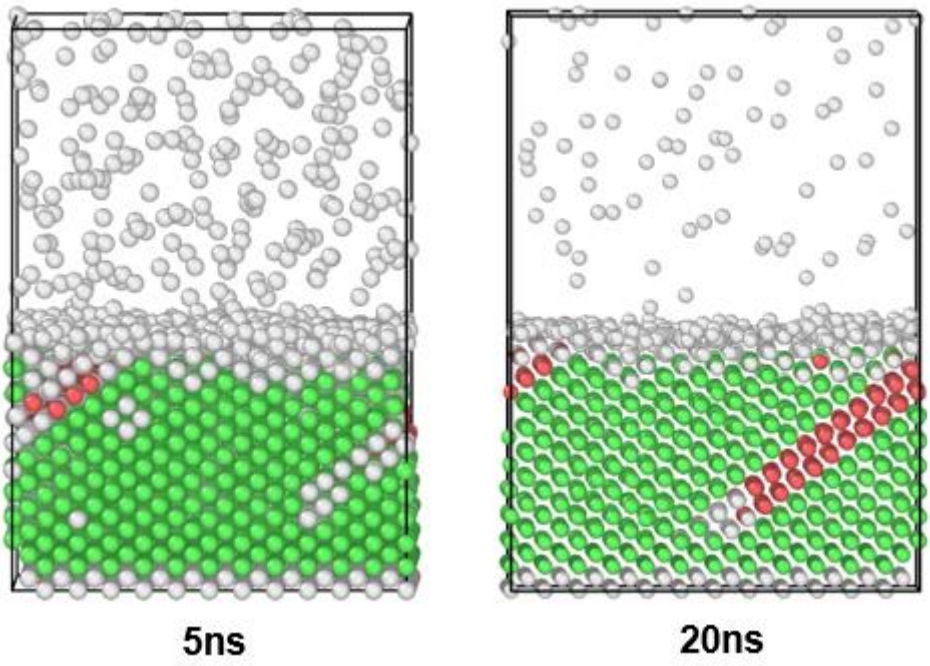

Figure 4-9 The result of the common neighbor analysis on the Ni/H_2O system

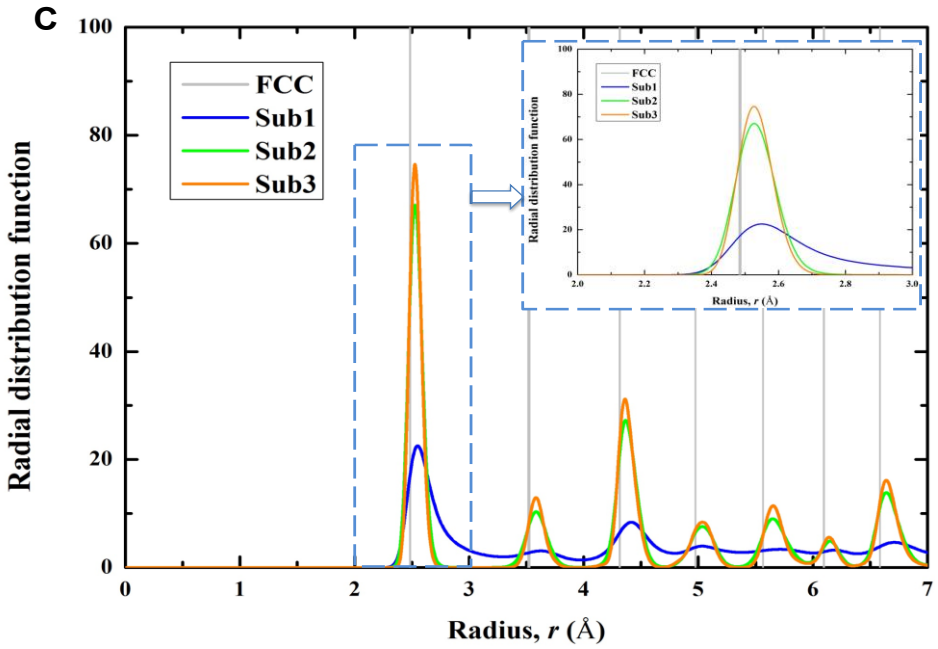

Figure 4-10 The results of Radial distribution function

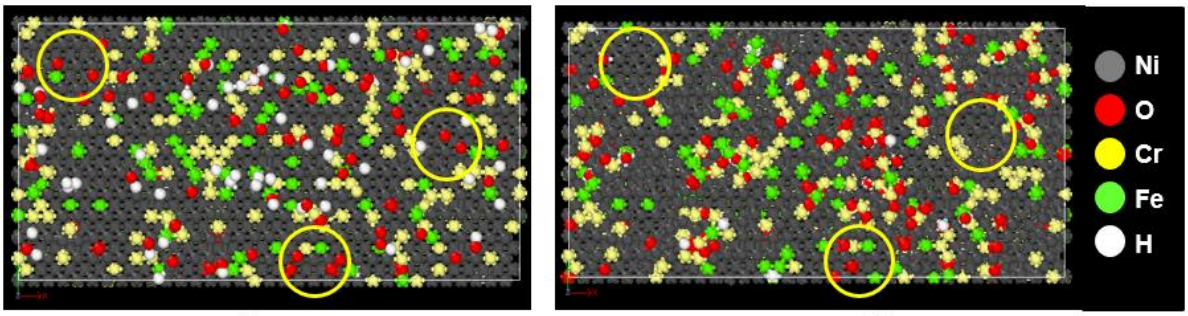

Figure 4-11 The result of Ni-15Cr-8Fe/H_2O system

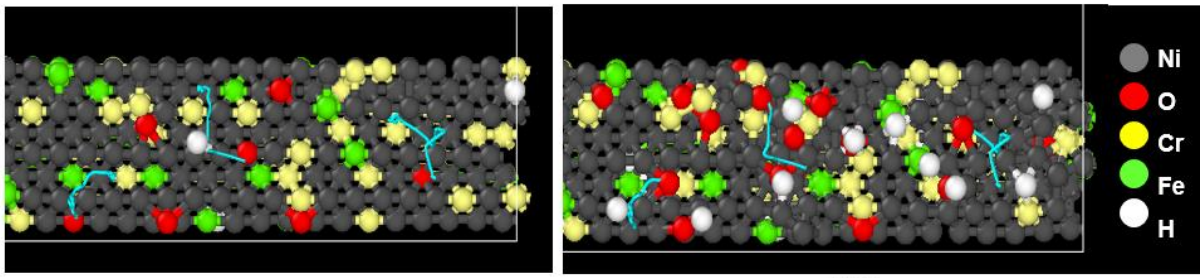

Figure 4-12 The trajectory of oxygen atom at the surface.

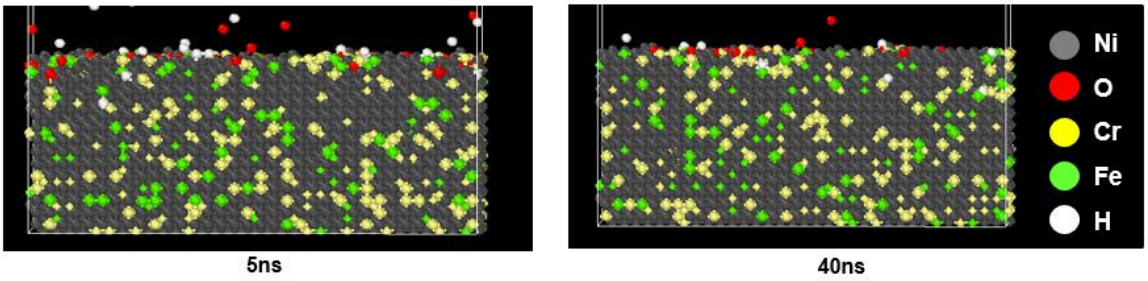

Figure 4-13 The final state of Ni-15Cr-8Fe/H_2O system

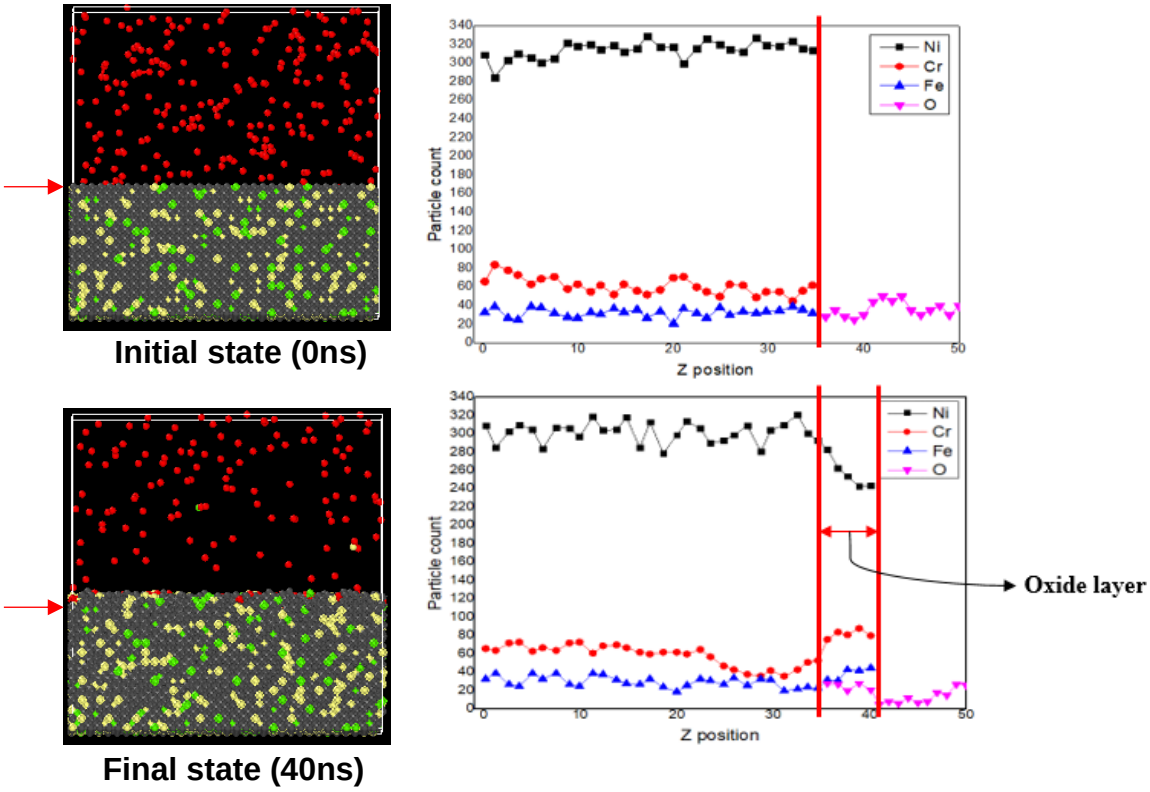

Figure 4-14 The results of oxidation layer analysis and atomic distribution diagram in the z-axis direction

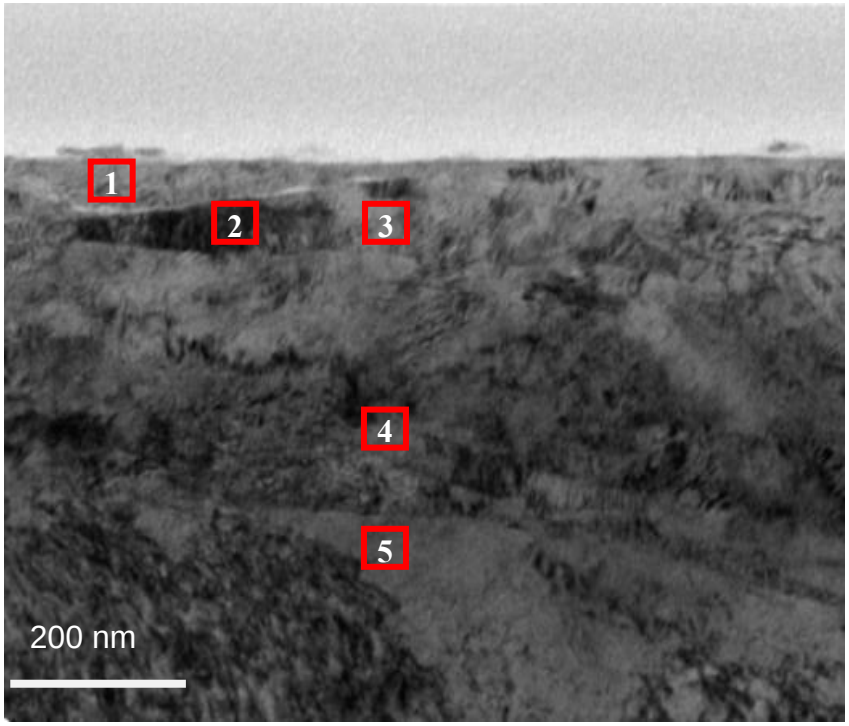

Figure 4-15 TEM images the surface on the Ni-15Cr-8Fe specimen

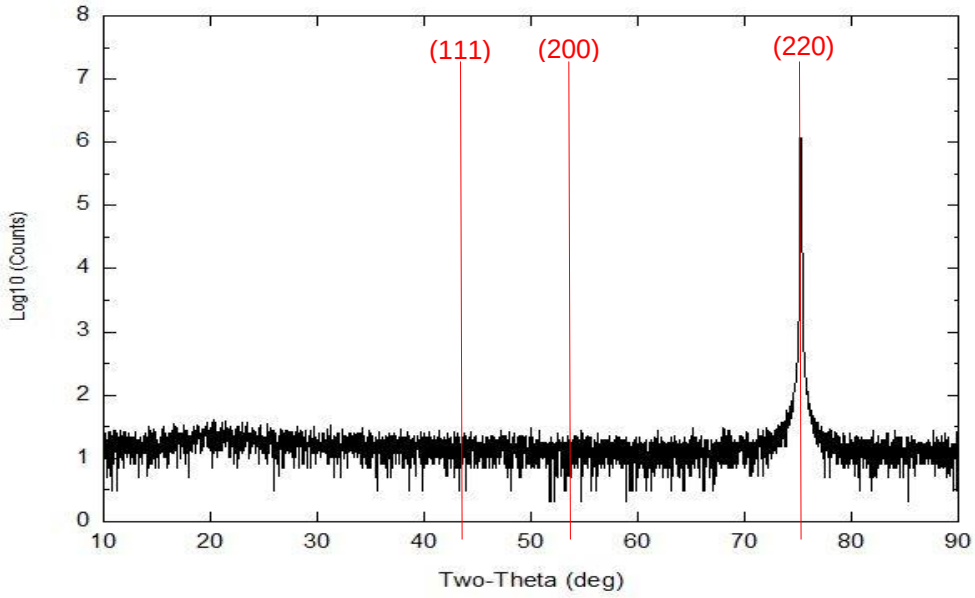

Figure 4-16 HRXRD results of Ni-15Cr-8Fe single crystal sample

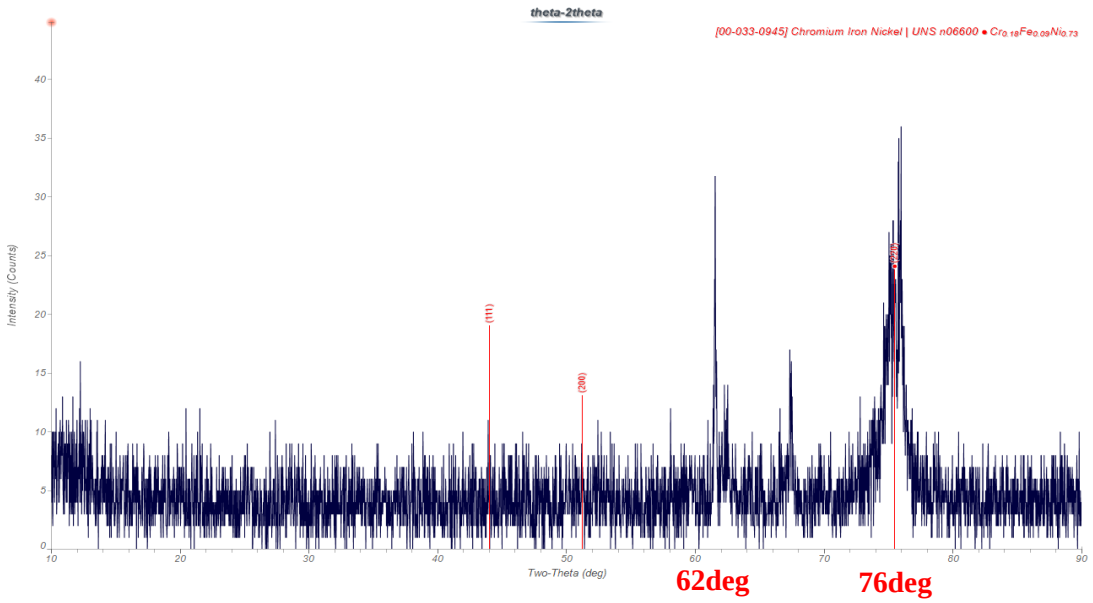

Figure 4-17 Powder X-ray diffraction results of Ni-15Cr-8Fe single crystal sample

5. Discussion

5.1. Atomistic structure of interfacial layer between nickel oxide and water

Some of the main causes of SCC are the content of alloying elements and misorientation of crystals such as grain boundaries. Since the correlation between grain boundary and SCC was presented by Watanabe, many studies have been conducted to understand how coincidence site lattice boundary and high angle boundaries affect SCC in the primary water environment [61,62]. These results show that the fractions of cracked grain boundaries decrease with increasing coincidence site lattice boundary fraction and HAB is more prone to cracks than coincidence site lattice boundary. Furthermore, cracks have been investigated to be easily propagated along HABs and deformable, and the direction of grain boundaries in applied stress has also been shown to be an important factor as shown in Figure 5-1 [63,64]. As such, grain boundaries have many effects on the oxidation process on metal surfaces. In this thesis analyzed surface structure based on results to investigate why grain boundaries are generated at the beginning of the oxidation process and how particle boundaries change.

Comparing the results of the first principle calculation and molecular kinetics calculations, Ni (111) surface forms the most stable phase when oxygen is adsorbed, but the diffusion of oxygen is slower than other surface structures due to the high barrier energy. In contrast, Ni (100) is less stable than the Ni (111) surface when oxygen is adsorbed, but the diffusion of oxygen is calculated to be the most advantageous. The molecular dynamics results show that the oxide film forms thickest at Ni (100). Therefore, even if adsorption occurs quickly, the formation of oxide layer can proceed slowly if diffusion path does not exist.

In the top view of the simulation cell in Figure 4-6, the atoms are initially ordered in hexagonal packing arrangements at the local scale (yellow rectangles), and the clusters agglomerate during relaxation to form larger domains (ordered yellow rectangles). However, some parts remain disordered persistently. The similar aspect appears in X-ray experiments. The crystal structures are arranged periodically in a three-dimensional space, which causes X-rays collide at the surface of the grid and scatter in a specific direction. This results in peaks with high intensity at certain angles, as shown by typical X-ray experiments.

However, amorphous phase does not have periodicity and is randomly distributed in three-dimensional space. When a diffraction experiment is performed at a relatively low angle, more amorphous phase can be observed in the mixture than the actual percentage and since X-rays are scattered in various directions, there is no clear diffraction pattern compared to crystal structure. Therefore, the peak with high intensity may not appear, such as a typical X-ray experiment, but a broad peak may appear over a broad range as shown in Figure 5-2 [32].

Being consistent with the XRR experiments, the simulation result shows a highly deformed interface, specifically as a result of the oxidation process. While previous studies only focused on the changes to the lateral structure due to the limited measurement tools, our simulations reveal that there are also substantial deformations in the surface normal direction. Amorphous and crystalline phases co-exist at the interface, suggesting complex growth processes caused by an intrinsic mismatch between the rectangular lattice of the NiO surface and the stable hexagonal packing of the NiO(111) epitaxy layer.

This structural change can provide a diffusion path because it is an unstable state in which continuous phase change occurs. This provides an environment in which crack can be produced on the oxide layer as shown in Figure 5-3.

5.2. The role of Cr atoms on oxidation characteristic of Ni based alloy

The describing the advantageous role of chromium atoms is complicated due to interaction of the various factors affecting SCC behavior. The main parameters also depend on the mechanisms considered to control the stress corrosion cracking mechanism. Also, the chromium atom is known as solid solution enhancer that can influence strain and creep of nickel based alloys. The creep decreased significantly as a result of Angeliu and Vaillant et al. (Figure 5-4) [42], whose compostion of chromium increased from 15 to 30 %. Chromium also influences formation of surface layer: increasing chromium content produces thin chromium-rich oxides in figure 5-5, 5-6 and 5-7 [43]. The oxide layer is also highly protective and has a higher mechanical resistance for chromium contents higher than 17 % [44]. In addition, repassivation and passivity rates have been indicated to composition of chromium increase [45, 46].

The effects of carbide distribution have been studied by several researchers [47-51], and the generally agree that semi-continuous or continuous network of intergranular precipitates of chromium carbides increased resistance of SCC, while carbide precipitation which located intergranular increases susceptibility of stress corrosion cracking in Figure 5-8 [51].

The nickel below the oxide layers has been found to exhibit two types of damage

1. Cr-depleted layer below the surface oxide
    - The presence of a Ni-rich layer below the surface oxide was directly observed by TEM/EDS on thin cross-sections transverse to the metal/solution interface.
2. Penetration of oxygen/oxide at the grain boundaries

- It has been observed that exposure to primary PWR coolant in the absence of applied stress causes irreversible embrittlement of Alloy 600 grain boundaries near the surface.

Some intergranular oxidation is also methodically observed on Alloy 600 and affects grain boundaries embrittlement, which is generally accepted as the cause of primary water stress corrosion cracking. In oxidizing water chemistry environments, there is no guarantee of sufficient protection by inner chromium rich oxide layer. The properties of the oxide layer remain uncertain in certain cases, and selective oxidation does not occur on the oxide/metal interface in alloy 600 where Cr_2O_3 presence and role are unclear. Therefore, it is important to find out the role of the chromium atom in the early stage oxidation process.

The oxidation reaction of a binary alloy (A and B) with aqueous water at high temperature can be written as

$$a\langle\langle A\rangle\rangle + b\langle\langle B\rangle\rangle + cH_2O \rightleftharpoons A_aB_bC_c + cH_{2<aq>} \quad (5.1)$$

The oxidation reactions, which were taken into account for the thermodynamic calculations, are the following figure 5-9 [52]. The Cr atoms can be concentrated on the surface due to the above phenomenon and Cr atom prevents oxygen atoms from spreading inside (Oxygen affinity : Ni < Cr) Also, this phenomenon could create a Cr deficiency phase under the surface oxide layer as shown in figure 4-9 ~ 4-11.

The X-ray diffraction experiments show that the Ni ternary crystal surface is mixed with amorphous layers and crystal with (110) oriented substrates during early stage oxidation. In addition, it has been confirmed that HCP crystal structure consisting of Ni_xO_y appears in areas where Cr does not exist such as Ni/water system. It is the same as the result confirmed by Ni/water system. As a result, two or more mismatches on the surface are expected to cause mutual stresses as shown in Figure 5-10.

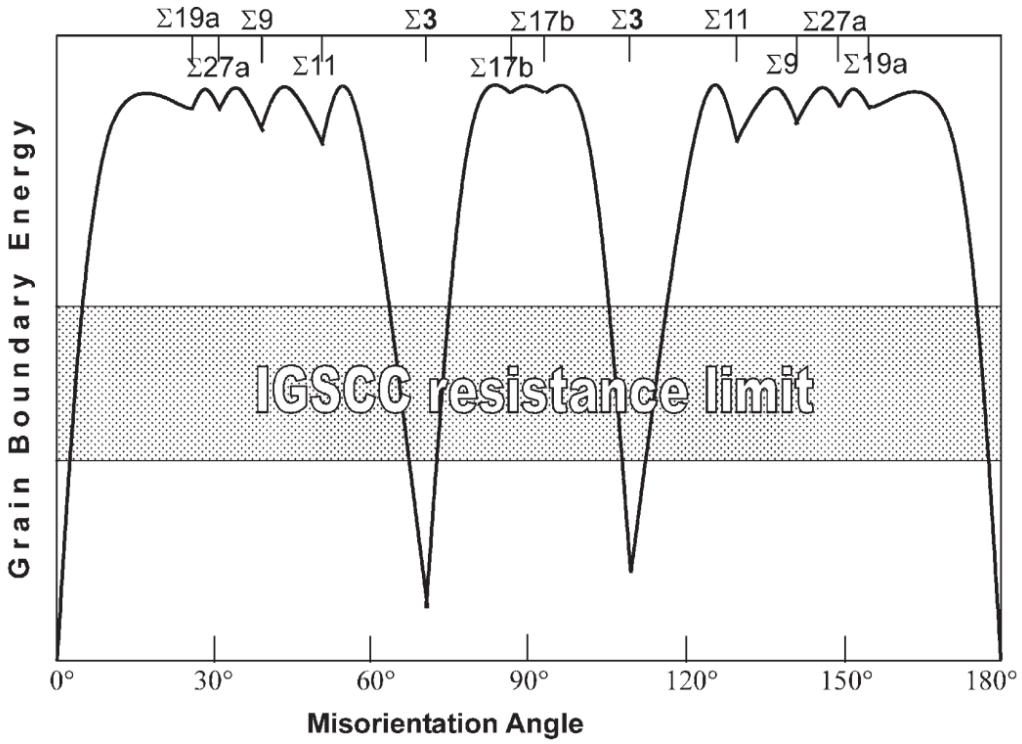

Figure 5-1 Schematic diagram represented an intergranular stress corrosion cracking resistance[61]

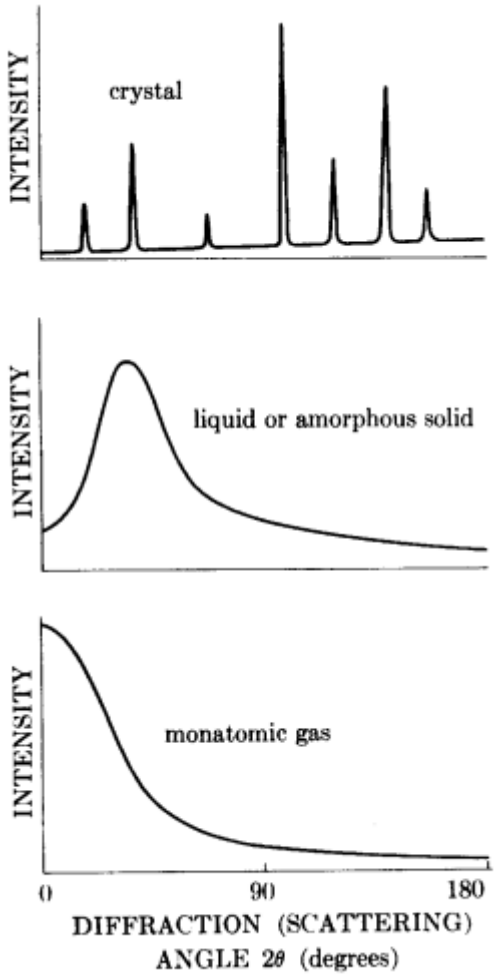

Figure 5-2 The schematic diagram of X-ray scattering characteristic by crystalline, amorphous, monatomic gases [32]

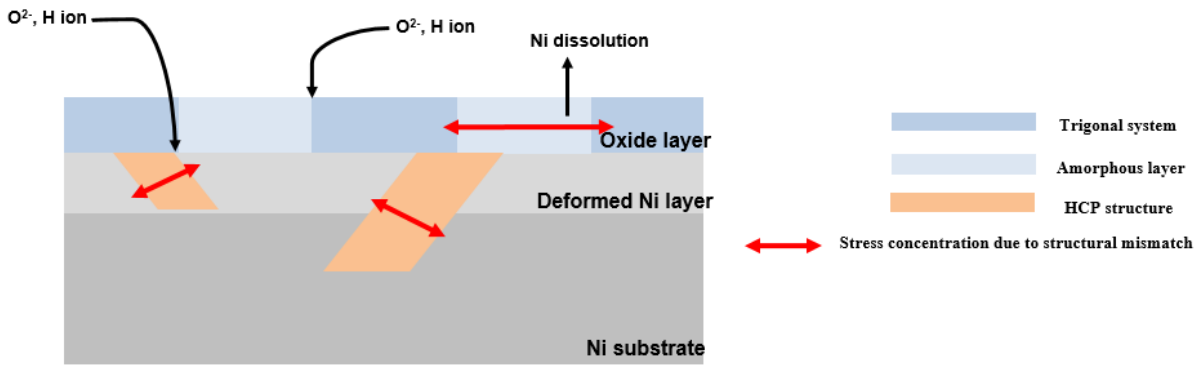

Figure 5-3 Schematic diagram of early stage oxidation mechanism in Ni/H_2O system

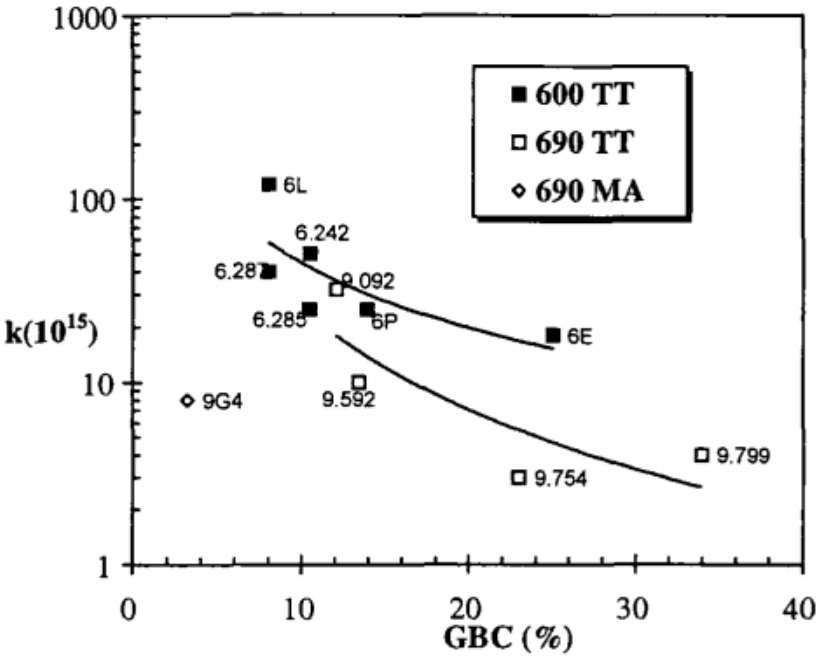

Figure 5-4 The difference of creep rate between alloy 600 and alloy 690 [42]

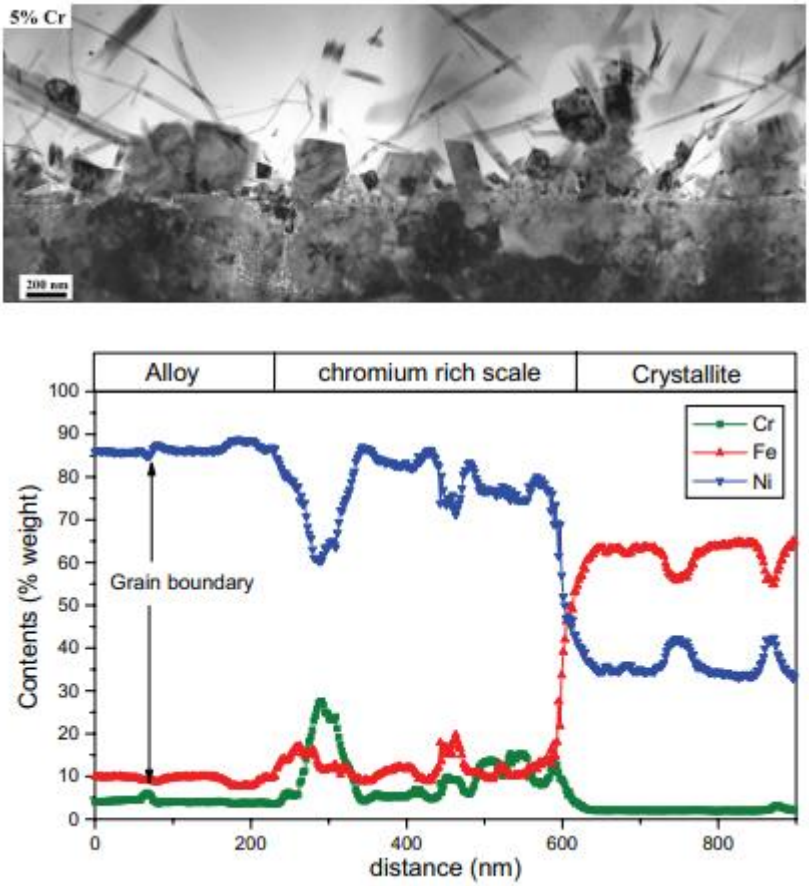

Figure 5-5 Transmission electron microscope cross-section of the oxide scale formed on the 5% Cr alloy in simulated primary water environment [43]

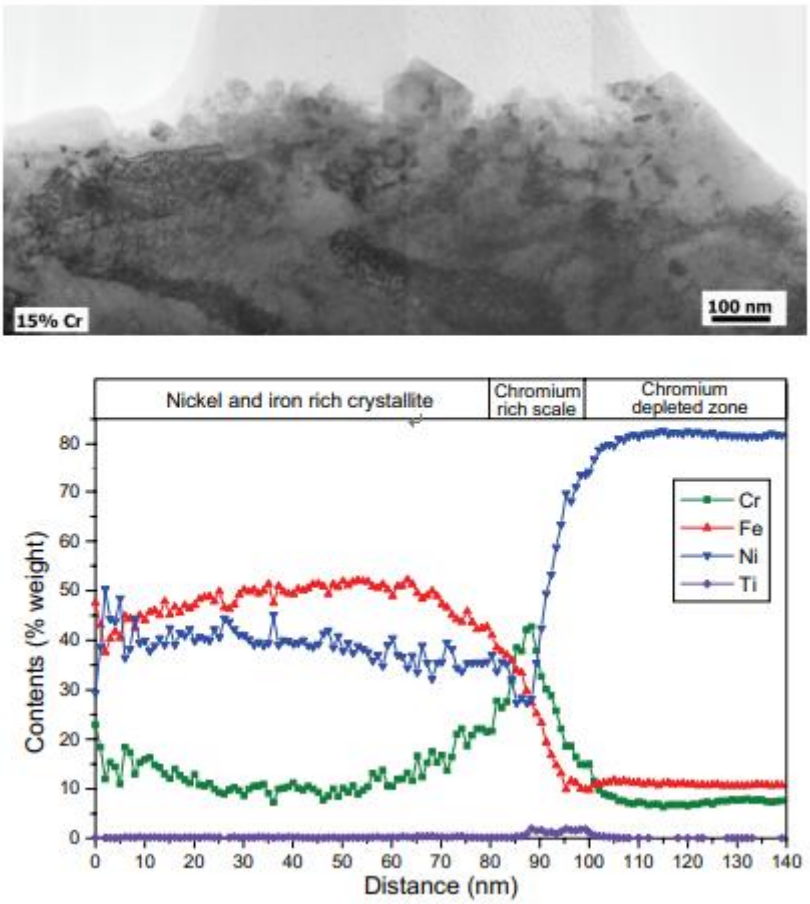

Figure 5-6 Transmission electron microscope cross-section of the oxide scale formed on the 15% Cr alloy in simulated primary water environment [43]

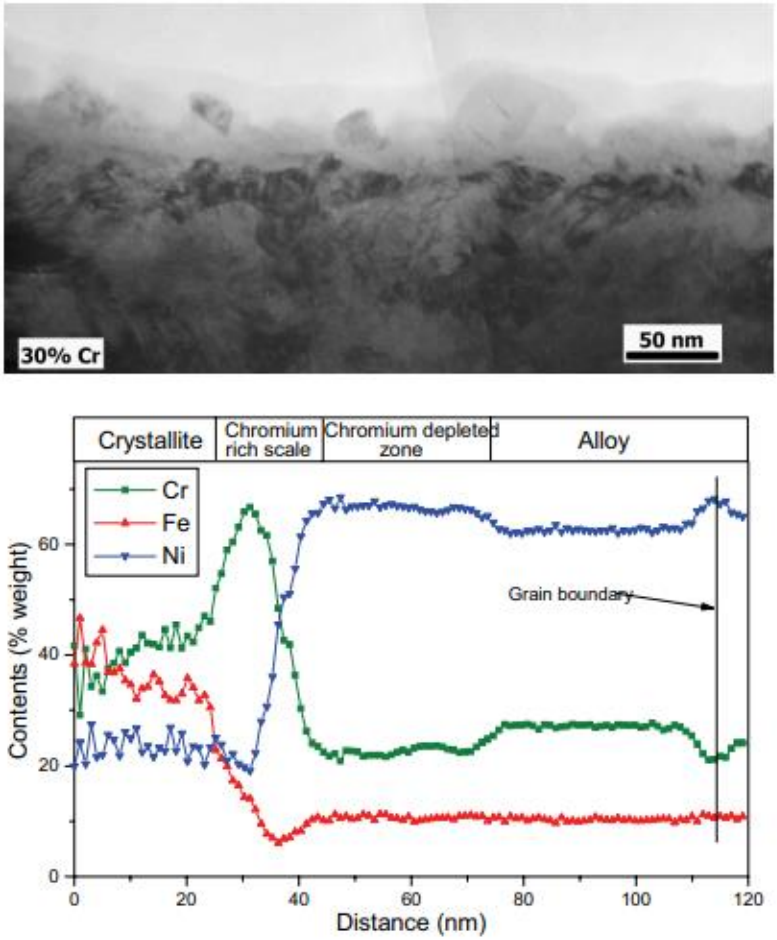

Figure 5-7 Transmission electron microscope cross-section of the oxide scale formed on the 30% Cr alloy in simulated primary water environment [43]

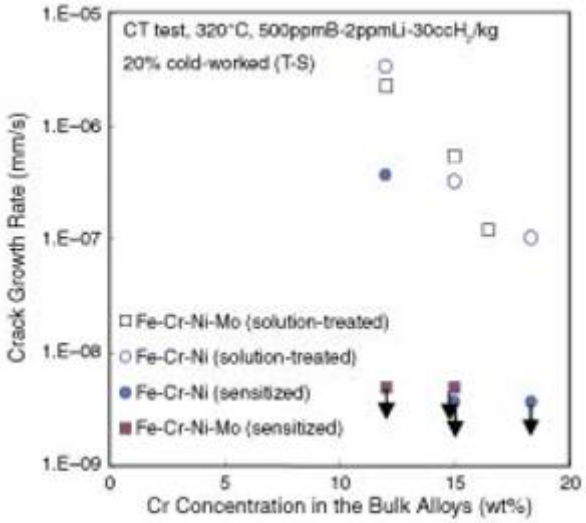

Figure 5-8 Effect of grain boundaries carbide on crack growth rate [51]

$$\langle\langle Ni\rangle\rangle + H_2O \rightleftarrows NiO + H_{2(aq)}$$
$$\langle\langle Cr\rangle\rangle + 3H_2O \rightleftarrows Cr_2O_3 + 3H_{2(aq)}$$
$$\langle\langle Ni\rangle\rangle + 2\langle\langle Cr\rangle\rangle + 4H_2O \rightleftarrows NiCr_2O_4 + 4H_{2(aq)}$$
$$\langle\langle Fe\rangle\rangle + 2\langle\langle Cr\rangle\rangle + 4H_2O \rightleftarrows FeCr_2O_4 + 4H_{2(aq)}$$
$$\langle\langle Ni\rangle\rangle + 2\langle\langle Fe\rangle\rangle + 4H_2O \rightleftarrows NiFe_2O_4 + 4H_{2(aq)}$$

$$Cr_2O_3 > FeCr_2O_4 > NiCr_2O_4 > NiFe_2O_4 > NiO$$

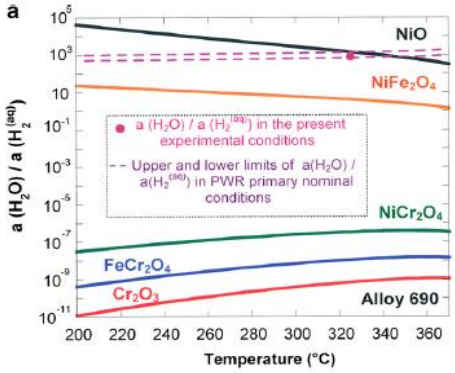

Figure 5-9 Stability diagram of the oxides which are likely to form during the exposition of alloy 600 in PWR primary water type media in function of temperature [52]

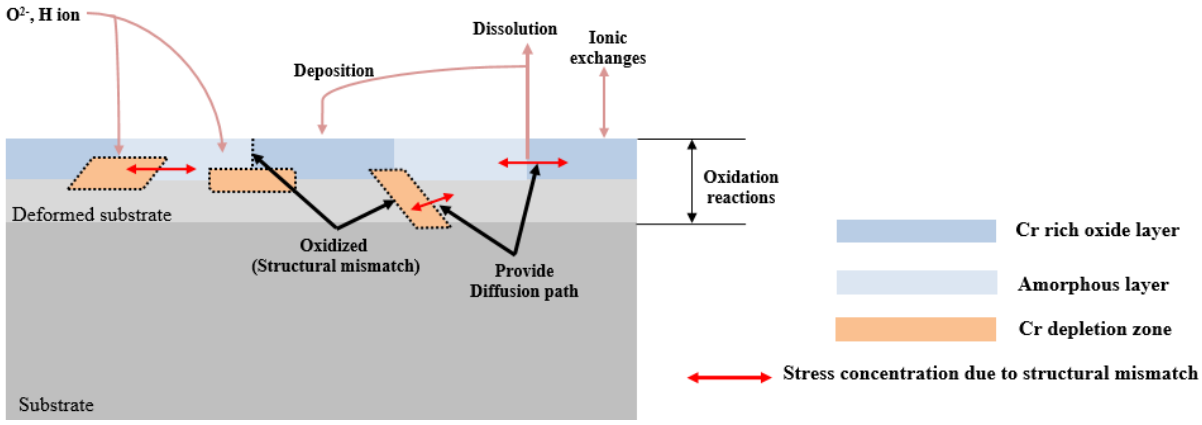

Figure 5-10 Schematic diagram of early stage oxidation mechanism in Ni-15Cr-8Fe/H_2O system

6. Conclusion

In this thesis, computational approaches and X-ray experiments were performed to understand the corrosion behavior mechanism of nickel based alloys at atomic unit scale during early stage oxidation. When oxidation begins, ionic changes occur at the metal/water interface. This phenomenon causes the dissolution of the metal atom and affects the growth of the oxide layer as it is deposition again. Therefore, the different phases coexist on the surface and this structural mismatch region can provide a diffusion path(metastable state) in which continuous phase change occurs. An environment is promoted in which crack can be formed by providing conditions for creating a brittle oxide film inside the oxide layer.

The high resolution x-ray experiments performed on the Ni (110) and Ni ternary single crystal/water interface to investigate the interface structure between the nickel oxide and the Ni single crystal substrate with atomic resolution. It was founded that the beating pattern at low Q values (0.5–2.0 $Å^{-1}$) which suggests there are at least two layers with different thicknesses. The beating pattern diminishes as Q increases, leaving only one epitaxial film Bragg peak at a higher Q. This suggests that one of the layers must be a non-epitaxial deposit. Being consistent with the simulation results, the XRR experiments show a highly deformed interface, specifically as a result of the oxidation process. In this result, We can see the importance of diffusion paths and how alloy elements affect crack production. And The proposed model can investigate the behavior of crack incubating and initiation steps that were insufficient in previous studies. We can also predict how this phenomenon affects crack initiation.

Following are the conclusion of this thesis;

1. Even if adsorption occurs quickly, the formation of oxide layer can proceed slowly if diffusion path does not exist. Diffusion path has a significant effect on oxide layer production.
2. The structural change of metal surface can provide a diffusion path because it is an unstable state in which continuous phase change occurs.
3. This environment is promoted in which crack can be formed by providing conditions for creating a brittle oxide film inside the oxide layer.

REFERENCE

[1] J.R. Davis, Nickel, Cobalt and their Alloys, ASM International Materials. 2000.

[2] Ballinger, R. F., Light Water Reactors: Materials of Construction and their Performance Characteristics that Impact Degradation, In: International conference on plants materials degradations: Application to the stress corrosion cracking of Ni base alloys. 2008.

[3] R.W. Staehle, The Theory of SCC in Alloys, II, NATO Science Committee, 1971, 279.

[4] A. Turnbull, Stress corrosion cracking: mechanisms, In K. H. Jürgen Buschow, Robert W. Cahn, Merton C. Flemings, and Bernard Ilschner, editors, Encyclopedia of Materials: Science and Technology. 2001, vol. 37, pp. 8886–8891.

[5] M.E. Gallagher, S. Haq, A. Omer, A. Hodgson, Water monolayer and multilayer adsorption on Ni(111), Sur. Sci. 2007, vol. 601, pp. 268-273.

[6] L.Olle, M. Salmeron, A.M. Baro, The adsorption and decomposition of water on Ni(110) studied by electron energy loss spectroscopy, J. Vac. Sci. Technol. 1985, vol. A3, pp. 1866-1870.

[7] Z. Peide, F.H. Stott, R. P. M. Procter, W.A. Grant, The early stages of oxidation of ion-implanted nickel at high temperature, Oxidation of Metals. 1981, vol. 16, pp. 409-426.

[8] V. P. Deodeshmukh, S.K. Srivastava, J. Bai, Early-stage oxidation behavior of Co-rich high temperature alloys, Materials and Corrosion. 2013, pp. 772-776.

[9] C. Lanthony, et al., On the early stage of aluminum oxidation: An extraction mechanism via oxygen cooperation, J. Chem. Phys. 2012, vol. 137.

[10] G.B. Hoflund, W.S. Epling, Oxidation study of a polycrystalline Ni/Cr alloy II, Chem. Mater. 1998, vol. 10, pp. 50-58.

[11] S.E. Ziemniak, M. Hanson. Corrosion behavior of NiCrFe alloy600 in high temperature, hydrogenated water, Corr. Sci. 2006, vol. 48, pp. 498-521.

[12] M. Juez-Lorenzo, V. Kolarik, W. Stamm, H. Fietzek, Oxidation of nickel-based alloys in dry and water vapour containing air, J. Mater, Sci. Tech. 2012, vol. 28, pp. 562-568.

[13] J. Kim et al., In-situ investigation of thermal aging effect on oxide formation in Ni-base alloy/low alloy steel dissimilar metal weld interfaces, 2014, Corr. Sci., vol. 86.

[14] J.Kim, K.J. Choi, C.H. Bahn, J.H. Kim, In-situ Raman spectroscopy analysis of surface oxide films on Ni-base alloy/low alloy steel dissimilar metal weld in high temperature water, J. Nucl. Matter. 2014, vol. 449, pp. 181-187.

[15] Z.P. Zhang, P. Li, Study on the trap site in Ni-Cr alloy by first principle approach, Vacuum. 2014, vol. 101, pp. 321-323.

[16] N.K. Das, T. Shoji, A density functional study of atomic oxygen and water molecule adsorption on Ni(111) and chromium-substituted Ni(111) surfaces, Appl. Surf. Sci. 2011, vol. 258, pp. 442-447.

[17] N.K. Das, I. Tirtom, T. Shoji, A multi-scale modeling study of a Ni-Cr(111) surface oxidation at different stress intensities, Mater. Chem. Phys. 2010, vol. 122, pp. 336-342.

[18] S.Garruchet, O.Politano, P. Arnoux, V. Vignal, Diffusion of oxygen in nickel : a variable charge molecular dynamics study. Solid state comm, 2010, vol. 150, pp. 439-442.

[19] C. Taylor, R.G. Kelly, M. Neurock, First principles calculations of the electrochemical reactions of water at an immersed Ni(111)/H2O interface, J. Electrochem. Soc. 2006, vol. 153, pp. 207-214.

[20] S. Yamagishi, S.J. Jenkins, D.A. King, First principles studies of chemisorbed O on Ni {111}, Surf. Sci. 2003, vol. 543, pp. 12-18.

[21] H. Coriou, L. Grall, Y. Legall, and S. Vettier, Stress corrosion cracking of Inconel in high temperature water, In Third Colloquium of Metallurgy. 1960, vol. 39, pp. 161.

[22] B. Grimmel and W.H. Cullen Jr, U.S. plant experience with Alloy 600 cracking and boric acid corrosion of light-water reactor pressure vessel materials, Technical Report NUREG-1823, Division of Engineering Technology Office of Nuclear Regulatory Research, Washington, DC, 2005. 39.

[23] Soustelle, C. et al., PWSCC of alloy 600: a parametric study of surface film effect, In Proc. 9th Int. Symp. On Environmental Degradation of Materials in Nuclear Power Systems – Water Reactors. 1999.

[24] T. Terachi et al., Influence of Dissolved Hydrogen on Structure of Oxide Film on Alloy 600 Formed in Primary Water of Pressurized Water Reactors, Journal of Nuclear Science and Technology. 2003, vol. 40, pp. 506-516.

[25] Koji DOZAKI et al., Effects of Dissolved Hydrogen Content in PWR Primary Water on PWSCC Initiation Property, E-Journal of Advanced Maintenance. 2010, vol. 2, pp. 65-76.

[26] P. Laghoutaris, J. Chêne, C. Guerre, O. Raquet, M. Sennour, R. Molins, F. Vaillant, and P. Scott, Contribution to understanding of stress corrosion cracking of alloy 600 in PWR primary water, Energy Materials: Materials Science and Engineering for Energy Systems. 2008, vol. 3, pp. 119–125.

[27] T. S. Gendron, S. J. Bushby, R. D. Cleland, and R. C. Newman, Oxidation embrittlement of alloy 600 in hydrogenated steam at 400 ◦C, In T. Magnin, editor, Corrosion-Deformation Interactions CDI '96: (EFC 21). CDI '96 in conjunction with Eurocorr '96, Maney Publishing. 1997, pp. 77-78.

[28] J. Panter, M. Foucault, J.-M. Cloué, P. Combrade, B. Viguier, and E. Andrieu, Surface layers on alloy 600 and 690 in primary water: possible influence on stress corrosion crack initiation, *In NACE International Corrosion 2002*. 2002, pp. 77-79.

[29] S. M. Bruemmer, Local deformation and IGSCC in LWR environments. Insights from crack-tip exams, In International conference on plant materials degradation - Application to the stress corrosion cracking of Ni-base alloys. EDF R&D centre of Les Renardières, Moret–Sur–Loing, France, 2008, pp. 78-79.

[30] J. Panter, B. Viguier, J.–M. Cloué, M. Foucault, P. Combrade, and E. Andrieu, Influence of oxide films on primary water stress corrosion cracking initiation of alloy 600, *Journal of Nuclear Materials*, 2006, vol. 348, pp. 213–221.

[31] P. Fenter, X-ray Reflectivity as a Probe of Mineral-Fluid Interfaces: A User Guide, Rev. Mineral, *Geochmistry*. 2002, vol. 49, pp. 149-221.

[32] B.D. Cullity, S.R. Stock, Elements of X-Ray Diffraction. 2nd ed.; Addison Weseley Publishing Company, Inc., MA, 1978.

[33] N.K. Das, T. Shoji, A density functional study of atomic oxygen and water molecule adsorption on Ni(111) and chromium-substituted Ni(111) surfaces, Appl. Surf. Sci. 2011, vol. 258, pp. 442-447.

[34] Xiaolong Liu et al., Atomistic investigation on initiation of stress corrosion cracking of polycrystalline Ni60Cr30Fe10 alloys under high-temperature water by reactive molecular dynamics simulation, Computational Materials Science, 2021, vol. 187.

[35] Robinson, I. K., Crystal truncation rods and surface roughness, Physical Review B, 1986, vol. 33, pp. 3830-3836.

[36] Farraro, R. & Mclellan, R. B., Temperature dependence of the Young's modulus and shear modulus of pure nickel, platinum, and molybdenum, Metallurgical Transactions A, vol. 8, pp. 1563-1565, doi:10.1007/bf02644859.

[37] Q.L. Tang, Z.X. Chen, Density functional slab model studies of water adsorption on flat and stepped Cu surfaces, Surface science, 601 (2007) 954.

[38] V. I. Avdeev, I. I. Zakharov, G. M Zhidomirov, N. M. Neshev, E. I. Proinov, Electronic structure of OH adsorbed on nickel, J. Struct. Chem, 1992, vol. 33, pp. 2.

[39] H. Tillborg, A. Nilsson, T. Wiell, N. Wassdahl, N. Martensson, J. Nordgren, Electronic structure of atomic oxygen adsorbed on Ni(100) and Cu(100) studied by soft X-ray emission and photoelectron spectroscopies, Phys. Rev. B, 1993, vol. 47, pp. 464-470.

[40] W.B. Zhang, B.Y. Tang, First-principles studies of the oxygen adsorption on unreconstructed and reconstructed Ni(110) surfaces, Surface science, 2009, vol. 603, pp. 1002-1009.

[41]

[42] F. Vaillant, J. D. Mithieux, O. de Bouvier, D. Vançon, G. Zacharie, Y. Brechet, and F. Louchet. Influence of chromium content and microstructure on creep and PWSCC resistance of nickel base alloys. Nineth international conference on environmental degradation of materials in nuclear power systems – water reactors, pp. 251, 1999.

[43] F. Delabrouille, L. Legras, F. Vaillant, P. Scott, B. Viguier, and E. Andrieu., Effect of the chromium content and strain on the corrosion of nickel based alloys in primary water of pressurized water reactors, In Twelfth international conference on environmental degradation of materials in nuclear power systems – water reactors, 2005.

[44] T. Yonezawa and K. Onimura. Effect of chemical compositions and microstructure on the stress corrosion cracking resistance of nickel-based alloys in high-temperature water. In International conference on evaluation of materials performance in severe environments, 1989, pp. 235.

[45] T. M. Angeliu and G. S. Was. The effect of chromium, carbon, and yttrium on the oxidation of nickel-base alloys in high temperature water. Journal of The Electrochemical Society, 1993, vol. 140, pp. 1877.

[46] K. Yamanaka and J. Murayama. In Fourth international conference on environmental degradation of materials in nuclear power systems – water reactors, 1989, 42.

[47] A. Aguilar, J. L. Albarran, H. F. Lopez, and L. Martinez. Microstructural response on the cracking resistance of alloy 600. Materials Letters, 2007, 61(1), pp. 274–277.

[48] J. M. Sarver, J. R. Crum, and W. L. Mankins. Effect of carbide precipitation on the corrosion behavior of Inconel alloy 690. In NACE International Corrosion 1987, San Francisco, California, U.S.A., March 1987. 4

[49] K. Norring, J. Engström, and P. Norberg. Intergranular stress corrosion cracking in steam generator tubing. Testing of Alloy 690 and Alloy 600 tubes. In Third international conference on environmental degradation of materials in nuclear power systems – water reactors, pages 587–593, Warrendale, Pennsylvania, August 1988. TMS (The Minerals, Metals & Materials Society).

[50] D. Gómez–Briceño, F. Blázquez, and F. Hernández. Influence of product type on stress corrosion cracking of alloy 600. Corrosion, 1999, 55(3):248–258.

[51] K. Arioka, et al. Influence of carbide precipitation and rolling direction on intergranular stress corrosion cracking of austenitic stainless steels in hydrogenated high-temperature water. Corrosion, 2006, 62.7: 568-575.

[52] M. Sennour, et al. A detailed TEM and SEM study of Ni-base alloys oxide scales formed in primary conditions of pressurized water reactor. Journal of nuclear materials, 2010, 402.2-3: 147-156.

[53] R. B. Rebak and Z. Szklarska–Smialowska. The mechanism of stress corrosion cracking of alloy 600 in high temperature water. Corrosion Science, 1996, 38(6):971–988.

[54] Scott, P. M., and M. Le Calvar. Some possible mechanisms of intergranular stress corrosion cracking of Alloy 600 in PWR primary water, Proc. 6th Int. Symp. on Environmental Degradation of Materials in Nuclear Power Systems–Water Reactors, 1993, 657-665.

[55] Delabrouille, Frédéric. Caractérisation par MET de fissures de corrosion sous contrainte d'alliages à base de nickel: influence de la teneur en chrome et de la chimie du milieu. Diss. 2004.

[56] Panter, Jerome, et al. Surface layers on alloys 600 and 690 in PWR primary water: possible influence on stress corrosion cracking initiation. CORROSION 2002, 2002.

[57] P. Scott, P. Combrade, and F. Vaillant. Selective oxidation at grain boundaries and internal oxidation. In International conference on plant materials degradation - Application to the stress corrosion cracking of Ni-base alloys, EDF R&D centre of Les Renardières, Moret–Sur–Loing, France, 2008.

[58] Eichler, A. CO adsorption on Ni(111): A density functional theory study. Surf. Sci. 2002, 526, 332-340

[59] Roques, J.; Anderson, A.B. Electrode potential-dependent stages in OH_{ads} formation on the Pt_3Cr alloy (111) surface. J. Electrochem. Soc. 2004, 151, E340-E347

[60] Roques, J.; Anderson, A.B. Theory for the Potential Shift of OH_{ads} Formation on the Pt Skin on Pt_3Cr(111)n Acid. J. Electrochemi. Soc. 2004, 151, E85-E91.

[61] V.Y. Gertsman, and Stephen M. Bruemmer. Study of grain boundary character along intergranular stress corrosion crack paths in austenitic alloys. Acta Materialia 2001, 49(9), 1589-1598.

[62] B. Alexandreanu, B. Capell, G.S. was. Combined effect of special grain boundaries and grain boundary carbides on IGSCC of Ni–16Cr–9Fe–xC alloys. Materials Science and Engineering: A, 2001, 300.1-2: 94-104.

[63] B. Alexandreanu, G.S. was. The role of stress in the efficacy of coincident site lattice boundaries in improving creep and stress corrosion cracking. Scripta materialia, 2006, 54.6: 1047-1052.

[64] V. Thaveeprungsriporn, G.S. was. Grain boundary properties of Ni-16Cr-9Fe at 360° C. Scripta materialia, 1996, 35.1.

Acknowledgement

학부생으로 UNIST 에 입학하여 대학원 졸업까지 어느새 11 년이 지났습니다. 아직도 부족한 점이 많지만 주위 많은 분들의 도움이 있어 이렇게 감사의 글을 쓸 수 있게 된 것 같습니다. 먼저, 어떻게 보면 생소할 지도 모르는 원자력 공학이라는 분야를 접하게 되고 첫 발을 디딜 수 있게 해주신 지도 교수님, 김지현 교수님께 먼저 감사 인사를 드립니다. 교수님께서 해주신 많은 지원과 조언 덕분에 어려운 난관을 넘기고 무사히 학위 과정을 마칠 수 있게 된 것 같습니다. 감사합니다. 그리고 바쁘신 와중에도 제 학위 논문 심사에 참석해 주신, 방인철 교수님, 권순용 교수님, 반치범 교수님, 윤의성 교수님께도 감사드립니다. 심사에 참석하여 주신 의견들과 개인적으로 찾아 뵈었을 때 해주신 말씀들은 연구를 돌아보고 마무리 하는데 있어 많은 도움이 되었습니다.

제가 이때까지 자라오는 동안 항상 믿어주시고 격려해주신 부모님께도 감사의 말씀을 드립니다. 어릴 때부터 타지에서 생활을 하게 되어 자주 보지는 못하지만 그래도 어떤 선택을 하던 응원해주시고 조언 해주셔서 잘 마무리할 수 있게 된 것 같습니다. 타지에 있어 잘 챙겨주지는 못하지만 동생 광석 에게도 감사의 마음을 전합니다. 글재주가 없어 표현은 못하지만 사랑하고 감사합니다.

몇 년 동안 매일 같이 함께 지낸 연구실 식구들에게도 감사의 글을 남깁니다. 김종진 박사님, 신상훈 박사님과 최경준 박사님, 처음 연구실 생활을 할 때 해주신 많은 조언들 항상 잊지 않겠습니다. 태호 형과 승현이 형도 학부생 때부터 정말 많은 일을 함께 겪고 도움도 많이 받았는데 그만큼 돌려줄 수 있을지는 모르겠지만 노력해 볼게요 항상 응원합니다. 그리고 연구실 동기들과 후배들도 좋은 일, 안좋은 일 함께 겪으며 오랜 시간 같이 지내 왔는데 항상 해오던 것처럼 앞으로도 서로에게 좋은 영향을 주는 관계가 되었으면 좋겠습니다. 마지막으로, 언제 만나도 어색하지 않고 아무 생각없이 같이

있기만 해도 마음이 편안한, 서로 힘든 일이 있으면 도와주던 친구들에게 감사의 인사를 전하며 감사의 글을 마칩니다.